HHS Public Access

Author manuscript

Science. Author manuscript; available in PMC 2022 May 05.

Published in final edited form as:

Science. 2021 November 05; 374(6568): eabe6723. doi:10.1126/science.abe6723.

Small proline-rich protein 2A is a gut bactericidal protein deployed during helminth infection

Zehan Hu[1,2,3,*,†], **Chenlu Zhang**[4,*], **Luis Sifuentes-Dominguez**[5], **Christina M. Zarek**[1], **Daniel C. Propheter**[1], **Zheng Kuang**[1], **Yuhao Wang**[1], **Mihir Pendse**[1], **Kelly A. Ruhn**[1], **Brian Hassell**[1], **Cassie L. Behrendt**[1], **Bo Zhang**[1], **Prithvi Raj**[1], **Tamia A. Harris-Tryon**[4], **Tiffany A. Reese**[1,†], **Lora V. Hooper**[1,2,†]

[1]Department of Immunology, University of Texas Southwestern Medical Center, Dallas, TX 75390, USA

[2]Howard Hughes Medical Institute, University of Texas Southwestern Medical Center, Dallas, TX 75390, USA

[3]Present address: State Key Laboratory of Microbial Metabolism, Joint International Research Laboratory of Metabolic and Developmental Sciences, School of Life Sciences and Biotechnology, Shanghai Jiao Tong University, Shanghai 200240, China

[4]Department of Dermatology, University of Texas Southwestern Medical Center, Dallas, TX 75390, USA

[5]Department of Pediatrics, University of Texas Southwestern Medical Center, Dallas, TX 75390, USA

Abstract

A diverse group of antimicrobial proteins (AMPs) helps protect the mammalian intestine from varied microbial challenges. Here, we show that small proline-rich protein 2A (SPRR2A) is an intestinal antibacterial protein that is phylogenetically unrelated to previously discovered mammalian AMPs. SPRR2A was expressed in Paneth cells and goblet cells and selectively killed Gram-positive bacteria by disrupting their membranes. SPRR2A shaped intestinal microbiota composition, restricted bacterial association with the intestinal surface, and protected against *Listeria monocytogenes* infection. SPRR2A was distinct from other intestinal AMPs by being induced by type 2 cytokines produced during helminth infection. Moreover, SPRR2A protected against helminth-induced bacterial invasion of intestinal tissue. Thus, SPRR2A is a unique AMP triggered by type 2 immunity that protects the intestinal barrier during helminth infection.

One-sentence summary:

[†]Corresponding authors: zehan.hu@sjtu.edu.cn, tiffany.reese@utsouthwestern.edu, lora.hooper@utsouthwestern.edu.
[*]These authors contributed equally to this work.

Author contributions:

Z.H., C.Z., T.A.H.-T., T.A.R., and L.V.H. designed research. Z.H., C.Z., L.S.-D., C.M.Z., D.C.P., Z.K., Y.W., M.P., K.A.R., B.H., C.L.B., B.Z., and P.R. performed research. Z.H., C.Z., L.S.-D., and P.R. analyzed data. Z.H., C.Z., T.A.R., and L.V.H wrote the paper.

Competing interests: Authors declare no competing interests.

SPRR2A is an intestinal antimicrobial protein that is induced by type 2 immunity and protects against bacterial invasion during helminth infection.

The mammalian intestine contains a complex community of microorganisms that present a diverse array of immunological challenges (1). This community is mostly composed of commensal bacteria that are essential for digestion but can also include opportunistic pathobionts and overtly pathogenic bacteria and fungi. In addition, the intestine can become infected with parasites such as helminths, a class of parasitic worms. Helminths can cause epithelial damage and provoke increased tissue invasion by intestinal bacteria (2, 3).

To cope with these varied microbiological challenges, the intestinal epithelium produces a diverse repertoire of antimicrobial proteins (AMPs), which have widely divergent primary sequences and rapidly kill or inactivate microorganisms (4, 5). Intestinal AMPs are secreted into the mucus layer that overlays the intestinal epithelium, where they restrict bacterial–epithelial contact and thus limit bacterial invasion of host tissues. One reason for the evolution of a diverse array of epithelial AMPs is that individual antimicrobial proteins target distinct populations of bacteria (e.g., Gram-positive versus Gram-negative bacteria), thus necessitating multiple AMPs to defend against challenges from complex bacterial populations.

A less well-explored idea is that a diverse AMP repertoire may also have evolved to provide antimicrobial protection in varied immunological settings. For example, helminth infections dramatically alter the immunological landscape of the intestine by triggering expression of type 2 cytokines such as interleukin (IL)-4 and IL-13 (6, 7). These cytokines direct numerous changes to epithelial cell function that promote worm expulsion, such as increased mucus secretion and turnover of epithelial cells (8, 9). However, little is known about how helminth infection and the ensuing production of type 2 cytokines shape the repertoire of epithelial AMPs, or which AMPs protect the host in the face of the dramatic helminth-induced alterations of the gut microbiota. Here, we identify small proline-rich protein A (SPRR2A) as an epithelial antibacterial protein, phylogenetically distinct from previously discovered mammalian AMPs, that plays a unique role in defending the intestinal barrier during helminth infection.

Results

SPRR2A is expressed in goblet cells and Paneth cells in the mouse intestine.

In a previous study, colonization of the germ-free mouse intestine with the Gram-negative commensal *Bacteroides thetaiotaomicron* elicited markedly increased expression of the gene encoding SPRR2A (10). SPRR2A belongs to the small proline-rich protein family of genes, which are encoded tandemly within a 170-kb region of the epidermal differentiation complex in both humans and mice (11). SPRR family genes are also induced during bacterial infection of the stomach, lung, and skin, suggesting a role in responding to infection (12–16). Although SPRRs have proposed functions in the development of the cornified envelope of squamous epithelia (17), virtually nothing is known about the

function of SPRR2A in the non-squamous intestinal epithelium and its role during bacterial colonization and infection.

In mice, *Sprr2a* transcripts were most abundant in tissues that interface with the external environment. These included the gastrointestinal tract, bladder, and skin (Fig. 1A and Fig. S1A). In the intestine, *Sprr2a* transcripts were selectively expressed in epithelial cells (IEC) (Fig. 1B), with expression of SPRR2A transcripts and protein restricted to secretory epithelial cell lineages including goblet cells and Paneth cells (Fig. 1, C to E, and Figs. S1, B and C, and S2, A to E). This accords with prior findings from single-cell RNA sequencing of the mouse small intestinal epithelium (fig. S1D) (18). SPRR2A was present in secretory granule-like structures within goblet cells and Paneth cells (Fig. 1F and fig. S1E), suggesting that SPRR2A might be secreted into the intestinal lumen. Supporting this idea, we detected SPRR2A in the stool and colonic mucus layer (Fig. 1G and fig. S1F). Thus, mouse SPRR2A is selectively expressed in intestinal secretory epithelial cells and is secreted into the intestinal lumen.

SPRR2A was also expressed in the human intestine. Several human colonic cell lines had abundant *SPRR2A* transcripts (table S1 and fig. S3, A and B) (19), and *SPRR2A* transcripts were detected in large intestinal biopsies from inflammatory bowel disease (IBD) patients but not healthy controls (table S2 and fig. S3C). Similar to mice, human SPRR2A was selectively localized to goblet cells (fig. S3D) and was detected in the stool of the IBD patients (fig. S3E).

We next examined the impact of the gut microbiota on SPRR2A expression in the small intestine. The prior study showing induction of *Sprr2a* expression upon *B. thetaiotamicron* colonization was conducted in germ-free NMRI mice, an outbred strain, and reported a ~200-fold increase in *Sprr2a* transcript abundance (10). By contrast, when we conventionalized germ-free C57BL/6 mice, we detected only a twofold increase in *Sprr2a* transcript abundance (fig. S4A). However, conventionalization of germ-free Swiss Webster mice resulted in a 20-fold increase (fig. S4A) and treatment of conventional BALB/c mice with broad-spectrum antibiotics reduced *Sprr2a* transcript abundance by ~50-fold (fig. S4A) with an accompanying decrease in protein levels (fig. S4, B and C). Notably, the *Sprr2a* transcript numbers in germ-free C57BL/6 mice were two orders of magnitude higher when compared to germ-free Swiss Webster mice or antibiotic-treated BALB/c mice (fig. S4D), which could explain why the induction of SPRR2A expression by the microbiota was less pronounced in C57BL/6 mice as compared to the other two strains. Additionally, monocolonization of germ-free mice with *Listeria monocytogenes* increased *Sprr2a* transcript abundance (fig. S4E). Thus, the microbiota induces intestinal expression of *Sprr2a*, but the magnitude of the increase varies according to mouse strain.

The microbiota-dependent increase in *Sprr2a* transcript abundance in C57BL/6 mice required the Toll-like receptor (TLR) signaling adaptor MyD88 (Fig. 1H). Accordingly, *Sprr2a* expression in germ-free mouse small intestine was triggered by lipopolysaccharide (LPS), a major component of the outer membrane of Gram-negative bacteria that activates TLR4-MyD88 signaling (Fig. 1I and fig. S4F). Thus, *Sprr2a* expression is induced by the intestinal microbiota through TLR–MyD88 signaling.

SPRR2A is a bactericidal protein that targets Gram-positive bacteria by membrane permeabilization.

SPRR2A has several characteristics that are shared with intestinal AMPs such as angiogenin-4 (ANG4), regenerating family member 3 gamma (REG3G), and resistin-like molecule beta (RELMβ) (20–23). These shared characteristics include expression in secretory epithelial cells and induction by bacterial colonization. Additionally, SPRR2A is basic, with a predicted isoelectric point of 8.4 (human) and 7.7 (mouse). This is also a shared characteristic of AMPs that target bacterial membranes, which are acidic due to the presence of negatively charged lipid headgroups (24). We therefore hypothesized that SPRR2A is an AMP.

To test for SPRR2A bactericidal activity, we produced recombinant human SPRR2A in insect cells and purified it by size exclusion chromatography (fig. S5, A and B). We added the purified SPRR2A to a panel of enteric commensal and pathogenic bacteria that included both Gram-positive and Gram-negative species (Fig. 2A and fig. S5C). We observed a dose-dependent reduction in the viability of the Gram-positive species *Lactobacillus reuteri, Enterococcus faecalis*, and *L. monocytogenes* when exposed to low micromolar concentrations of SPRR2A. By contrast, the Gram-negative species *B. thetaiotaomicron, Escherichia coli*, and *Citrobacter rodentium* were resistant to SPRR2A (Fig. 2A and fig. S5C). SPRR2A bactericidal activity against Gram-positive bacteria was inhibited by an anti-SPRR2A polyclonal antibody, indicating that the bactericidal activity was specific to the SPRR2A protein (Fig. 2B). Thus, SPRR2A is a bactericidal protein that selectively kills Gram-positive bacteria.

Similar to other intestinal AMPs, the bactericidal activity of SPRR2A required low salt concentrations and an acidic pH (fig. S5, D and E) (23, 25). This accords with the fact that intestinal AMPs such as SPRR2A must function in the acidic, low-salt environment of the mucus layer and intestinal lumen (26). Unlike other AMPs such as RELMβ (23), the bactericidal activity of SPRR2A was not dependent on the growth phase of the target bacteria, as SPRR2A killed logarithmic-phase and stationary-phase bacteria with similar efficiency (fig. S5F).

To acquire initial insight into how SPRR2A kills bacteria, we used transmission electron microscopy to visualize morphological changes in Gram-positive bacteria after exposure to SPRR2A. The images showed evidence of bacterial cell wall damage and cytoplasmic leakage (Fig. 2C and fig. S5G), suggesting that SPRR2A kills bacteria by permeabilizing their membranes. To test this idea, we measured bacterial membrane permeabilization by assaying for bacterial uptake of propidium iodide (PI), a membrane-impermeant dye. SPRR2A promoted the dose-dependent uptake of PI by *L. monocytogenes, L. reuteri* and *E. faecalis* but not by *B. thetaiotaomicron* (Fig. 2D and fig. S6A). Membrane permeabilization by SPRR2A required low salt concentrations and an acidic pH (fig. S6, B and C), consistent with the requirements for bactericidal activity. Thus, SPRR2A kills bacteria by disrupting their membranes.

The requirement for low salt concentrations and an acidic pH suggested that electrostatic interactions might be driving SPRR2A interactions with bacterial membranes, which tend

to be acidic (24). In support of this idea, we found that SPRR2A bound selectively to immobilized lipids bearing negatively charged lipid head groups, including phosphatidic acid (PA), phosphatidylserine (PS), cardiolipin (CL), and phosphatidylinositol phosphates (PIPs), but not to zwitterionic or neutral lipids (Fig. 2E). Moreover, SPRR2A was precipitated by liposomes containing negatively charged phosphatidylserine or cardiolipin, but not by liposomes composed of only the neutral lipid phosphatidylcholine (PC) (Fig. 2F). These interactions were also salt- and pH-dependent (fig. S6, D and E), supporting the concept that electrostatic interactions drive SPRR2A–lipid interactions. Thus, SPRR2A binds to lipids bearing negatively charged headgroups that reflect the acidic characteristic of most bacterial membranes.

To test whether SPRR2A disrupts membranes, we added purified SPRR2A to liposomes. Liposomes that were exposed to SPRR2A and visualized by negative-stain electron microscopy were completely disrupted, with only membrane fragments remaining (Fig. 2G). We next conducted dye efflux assays on liposomes encapsulating fluorescent dyes of different sizes. SPRR2A induced rapid dye efflux from PC/PS and PC/CL liposomes loaded with either carboxyfluorescein (~10-Å Stokes diameter) or fluorescein isothiocyanate-dextran 10 (~44-Å Stokes diameter) (Fig. 2H and fig. S6, F to H), indicating a lack of size selectivity in SPRR2A-induced dye efflux. There was no dye efflux from liposomes composed only of PC (Fig. 2H). By contrast, the microbiota-inducible intestinal AMPs REG3A and RELMβ form structured pores that are visible by negative-stain electron microscopy and which induce size-selective dye efflux from liposomes (23, 27). Thus, SPRR2A disrupts membranes but uses a mechanism that is distinct from that of other known microbiota-inducible AMPs.

The SPRR2A-mediated killing of *L. monocytogenes* was inhibited by LPS (Fig. 2I), suggesting that the resistance of Gram-negative bacteria may be due to the LPS in their outer membranes. LPS did not inhibit SPRR2A binding to either Gram-positive or Gram-negative bacteria or to PC:PS liposomes (fig. S7, A to C), arguing against binding interference as the mechanism of inhibition. Rather, LPS inhibited SPRR2A disruption of liposomes (Fig. 2J and K). Thus, LPS appears to inhibit SPRR2A bactericidal activity by interfering with membrane permeabilization.

Many proline-rich proteins are intrinsically unstructured due to proline's disruptive effect on secondary structures such as α-helices and β-sheets (28). However, in addition to being proline-rich, SPRR2A is also cysteine-rich (fig. S8), with 11 cysteines that form five pairs of intrachain disulfide-bonds (fig. S9, A and B). Since disulfide bonds can impart higher-order structure to proteins, we assessed whether the disulfide bonds were essential for SPRR2A bactericidal function. The bactericidal activity of SPRR2A was inhibited by the reducing agent 1,4-dithiothreitol (DTT) (fig. S9C), indicating that the disulfide-bonds are required for SPRR2A bactericidal activity. Consistent with this finding, DTT also inhibited lipid binding by SPRR2A (fig. S9, D to F). Finally, SPRR2A purified from *E. coli* (fig. S9D), which does not support the formation of disulfide bonds, did not bind negatively charged lipids, disrupt liposomes, or kill Gram-positive bacteria (fig. S9, E, G and H). Thus, disulfide bonds are necessary for lipid binding and bacterial killing by SPRR2A.

Mice lacking SPRR2A have an altered intestinal microbiota and are more susceptible to *Listeria monocytogenes* infection.

The bactericidal activity of SPRR2A suggested that it might regulate intestinal microbiota composition, contact between bacteria and the intestinal surface, and/or pathogen colonization. To test for these effects in vivo, we created mice lacking SPRR2A. Mice have three copies of the *Sprr2a* gene *(Sprr2a1, Sprr2a2*, and *Sprr2a3*), which all encode the same protein (fig. S2A and fig. S8). We therefore used CRISPR/Cas9-mediated gene targeting to delete the entire mouse *Sprr2a* locus (fig. S2, A and B), and verified that *Sprr2a*$^{-/-}$ mice lacked SPRR2A transcript and protein expression (fig. S2, C to E). *Sprr2a*$^{-/-}$ mice were born in normal Mendelian ratios, were healthy when reared in a specified-pathogen-free (SPF) facility, and showed normal intestinal morphology with no signs of inflammation (fig. S10A) and no increased paracellular permeability (fig. S10B).

Although overall small intestinal bacterial loads in wild-type and *Sprr2a*$^{-/-}$ littermates were similar (fig. S10C), 16*S* rRNA gene sequencing analysis of male wild-type and *Sprr2a*$^{-/-}$ littermates revealed an increased abundance of Gram-positive bacteria in the small intestinal lumen of *Sprr2a*$^{-/-}$ mice, with a marked increase in the relative abundance of *Lactobacillus, Turicibacter*, and *Candidatus Arthromitis* (segmented filamentous bacteria, or SFB, belonging to the class *Clostridia*). At the same time, there was a reduction in the abundance of *Bacteroidetes*, a class of Gram-negative bacteria (Fig. 3, A to C, and fig. S10D). We observed similar microbiota alterations in both male and female wild-type and *Sprr2a*$^{-/-}$ littermates under different caging conditions (fig. S11, A to F), indicating that the alterations were not caging- or sex-dependent. The microbiota composition in the colonic lumen was similar between *Sprr2a*$^{-/-}$ mice and their wild-type littermates (Fig. 3, A to C). This may reflect the increased density of the bacterial communities in the colon, or the increased rigidity and thickness of the colonic mucus layer when compared to the small intestinal mucus layer (29), which could limit the effect of a single AMP deficiency on the whole microbial community. These small-intestinal phenotypes are consistent with our finding that SPRR2A selectively kills Gram-positive bacteria (Fig. 2A) and indicate that SPRR2A shapes the composition of bacterial communities in the small-intestinal lumen.

A key function of other microbiota-inducible intestinal antimicrobial proteins is to limit contact between bacteria and the intestinal epithelial surface by restricting bacterial colonization of the mucus layer that overlays the intestinal epithelium (22, 23). When analyzing mucus-associated bacteria in the small intestine, we detected an increase in the abundance of the Gram-positive SFB and a decrease in the abundance of the Gram-negative *Bacteroidetes* (Fig. 3, A and C). The differences in mucus-associated bacteria were confined to the small intestine, as we did not detect marked differences in the composition of mucus-associated bacterial communities in the colon (Fig. 3, A and C). Finally, visualization of bacteria in the small intestinal mucus layer showed more bacteria in close association with the epithelial surface of *Sprr2a*$^{-/-}$ mice than wild-type mice (Fig. 3D). The filamentous morphology of the surface-associated bacteria in *Sprr2a*$^{-/-}$ mice (Fig. 3D) suggested that they were mostly SFB, consistent with the compositional analysis of mucus-associated bacteria (Fig. 3, A and C). Thus, SPRR2A regulates Gram-positive colonization of the

small intestinal mucus layer and limits interactions between bacteria and the small intestinal surface.

We next assessed the susceptibility of *Sprr2a*$^{-/-}$ mice to infection with a bacterial pathogen. Oral infection of *Sprr2a*$^{-/-}$ mice with the Gram-positive pathogen *L. monocytogenes* resulted in higher bacterial burdens in mesenteric lymph nodes, liver, and spleen as compared to wild-type mice (Fig. 3E). *Sprr2a*$^{-/-}$ mice also showed higher mortality following a high-dose oral *L. monocytogenes* infection (Fig. 3F). Thus, SPRR2A protects against infection by a Gram-positive bacterial pathogen in vivo.

SPRR2A expression is induced by type 2 cytokines during helminth infection of the intestine.

Helminth infections can cause numerous pathologies, including damage to the intestinal epithelium, which promotes bacterial breach of the intestinal barrier (3) and underscores the need for AMP expression. Prior studies have shown that SPRR2A expression increases markedly during intestinal infection by parasitic helminths such as *Trichinella spiralis, Nippostrongylus brasiliensis*, and *Heligmosomoides polygyrus* (30–32). Accordingly, the abundance of *Sprr2a* transcripts increased in the duodenum and proximal jejunum when we infected C57BL/6 and BALB/c mice with *H. polygyrus* (Fig. 4A and fig. S12). The magnitude of the change was greater in BALB/c than in C57BL/6 mice (Fig. 4A and fig. S12), likely due to the higher baseline levels of SPRR2A expression in C57BL/6 mice (fig. S4D). The increase in SPRR2A expression was less pronounced in the ileum and colon (fig. S12), consistent with the fact that *H. polygyrus* resides predominantly in the duodenum and proximal jejunum of mice. After helminth infection, there were more SPRR2A-producing goblet cells in the jejunum and SPRR2A expression in individual cells was also increased (Fig. 4B). Additionally, helminth-induced SPRR2A expression was maintained in antibiotic-treated mice and was therefore independent of the intestinal microbiota (fig. S13, A and B). Thus, helminth infection induces SPRR2A expression above the levels elicited by bacterial colonization.

Since helminth infection induces strong type 2 immunity in the intestinal tract, we asked whether SPRR2A expression is induced by type 2 cytokines such as IL-4 or IL-13. We first addressed this question using small-intestinal organoids, which are established from Lgr5^{+} stem cells and develop all of the epithelial cell lineages of the in vivo mouse epithelium (33). SPRR2A expression increased when organoids from wild-type C57BL/6 small intestines were exposed to IL-4 and IL-13, but not when exposed to other cytokines, including IFN-γ, IL-1β, and IL-22 (Fig. 4C). Intraperitoneal injection of IL-13, but not IL-22, into wild-type BALB/c mice also increased expression of SPRR2A in the small intestine (Fig. 4D), demonstrating that a type 2 cytokine can induce SPRR2A expression in vivo. Thus, type 2 cytokines increase SPRR2A expression in the small intestine.

IL-4 and IL-13 induce type 2 immunity during helminth infection through the transcription factor STAT6. We therefore studied *Stat6*$^{-/-}$ mice to further assess the involvement of type 2 cytokines in boosting *Sprr2a* expression during helminth infection. Although *H. polygyrus* infection elicited a ninefold increase in *Sprr2a* transcript abundance in the proximal jejunum of wild-type C57BL/6 mice, there was no increase in *Sprr2a* transcript abundance in infected

Stat6$^{-/-}$ mice (Fig. 4E). However, microbiota-dependent baseline expression of *Sprr2a* was maintained in *Stat6*$^{-/-}$ mice (fig. S13C). Thus, type 2 cytokines and their downstream signaling pathways induce *Sprr2a* expression during helminth infection but are not required for baseline induction of *Sprr2a* expression by the microbiota.

SPRR2A protects against helminth-induced bacterial invasion of intestinal tissue

We next assessed the impact of SPRR2A on intestinal helminth infection and the ensuing type 2 immune response. Intestinal worm burden and egg counts were similar in wild-type and *Sprr2a*$^{-/-}$ mice after *H. polygyrus* infection (Fig. 5A). Additionally, markers of intestinal type 2 immunity, including *Il13* expression, goblet cell numbers, and tuft cell numbers, were increased in both wild-type and *Sprr2a*$^{-/-}$ mice (fig. S14, A to F). Thus, SPRR2A does not directly affect the ability of *H. polygyrus* to establish an infection, nor does it alter the type 2 immune response. However, it remains possible that SPRR2A could impact worm fitness or expulsion at later timepoints.

Although *H. polygyrus* infection increased *Sprr2a* expression in the small intestine, there was decreased expression of transcripts encoding other AMPs, including REG3B, REG3G, lysozyme, intelectin-1, and several α-defensins (Fig. 4A and fig. S15), consistent with prior findings (32). This suggested that SPRR2A may be essential for defense of the intestinal barrier during *H. polygyrus* infection. To test this idea, we infected wild-type and *Sprr2a*$^{-/-}$ mice with *H. polygyrus* for 2 weeks and then assessed bacterial burdens in host tissues. Immunofluorescence and 16*S* quantitative PCR analysis of *H. polygyrus*-infected *Sprr2a*$^{-/-}$ mice revealed more bacteria in intestinal tissues than in infected wild-type mice (Fig. 5, B and C), and higher bacterial burdens in *Sprr2a*$^{-/-}$ mesenteric lymph nodes (Fig. 5C). The tissue-associated bacteria in *Sprr2a*$^{-/-}$ mice were characterized by an increased abundance of Gram-positive *Bacilli* and a decreased abundance of Gram-negative *Bacteroidia* (fig. S16, A to D), consistent with the selective killing of Gram-positive bacteria by SPRR2A in vitro (Fig. 2A). Thus, SPRR2A is essential for resistance to bacterial invasion of intestinal tissues during *H. polygyrus* infection (fig. S17).

Discussion

Here we have identified SPRR2A as an intestinal antibacterial protein that is unrelated to any previously discovered mammalian AMP. Other SPRR proteins are expressed in the lung and skin of mice and humans and are induced by infection, thus suggesting that SPRR2A may be representative of a previously unknown family of AMPs that defend mammalian body surfaces.

Although this is the first report of bactericidal activity in a member of the SPRR family, other proline-rich AMPs, unrelated to the SPRR family, have been identified in flies, frogs, cows, and sheep, but not in mice or humans (34). These proteins selectively target Gram-negative bacteria and use a different mechanism of bacterial killing that involves translocation across the bacterial membrane and inhibition of specific cellular processes in bacterial cells. Thus, SPRR2A is unique relative to previously characterized proline-rich AMPs by disrupting bacterial membranes and selectively targeting Gram-positive bacteria.

SPRR2A contributes to intestinal innate immunity by shaping microbiota composition, restricting bacterial access to host tissues, and by limiting infection by the Gram-positive bacterial pathogen *L. monocytogenes*. A unique aspect of SPRR2A function is its essential role in defending the intestinal barrier against bacterial invasion during helminth infection. Although helminth infection lowers the expression of a number of intestinal AMPs, SPRR2A expression is selectively increased by the type 2 cytokines that are abundantly produced during helminth infection. At the same time, RELMβ, which preferentially kills Gram-negative bacteria, is also upregulated following *H. polygyrus* infection (Fig. 4A and fig. S15) (23, 32, 35). This suggests that SPRR2A may work in concert with RELMβ to kill both Gram-positive and Gram-negative bacteria and thus maintain the intestinal barrier during helminth infection. The elevated production of these two antibacterial proteins during helminth infection could help to explain how helminth-infected mice resist colonization by bacteria that promote inflammation (36). These findings also illuminate how different AMPs may be deployed in distinctive immunological settings and provide insight into why a diverse repertoire of AMPs has evolved to defend the intestine.

Materials and Methods

Mice

Conventionally raised C57BL/6 wild-type, *Sprr2a*$^{-/-}$, *Myd88*$^{-/-}$ (37), and *Stat6*$^{-/-}$ mice (38), and conventionally raised BALB/c wild-type mice were bred and maintained in the SPF barrier facility at the University of Texas Southwestern Medical Center at Dallas. The generation of *Sprr2a*$^{-/-}$ mice is described below. *Stat6*$^{-/-}$ mice (38) were acquired from Jackson Laboratory (stock number: 005977; B6.129S2(C)-*Stat6*^{tm1Gru}/J and stock number: 002828; C.129S2-*Stat6*^{tm1Gru}/J). Germ-free C57BL/6 wild-type and *Myd88*$^{-/-}$ mice and Swiss Webster wild-type mice were bred and maintained in the gnotobiotic mouse facility at the UT Southwestern Medical Center. All mice were housed under a 12-hour-light:12-hour-dark cycle. Mice were fed ad libitum with free access to drinking water according to protocols approved by the Institutional Animal Care and Use Committees (IACUC) of UT Southwestern Medical Center.

Sprr2a$^{-/-}$ mice lacking all three mouse *Sprr2a* genes (*Sprr2a1, Sprr2a2*, and *Sprr2a3*) were generated using CRISPR/Cas9 genome editing with guide RNAs that targeted regions upstream and downstream of the *Sprr2a* locus (fig. S2, A to E). Guide RNAs were injected into fertilized C57BL/6J embryos along with in vitro transcribed Cas9 mRNA by the UT Southwestern Transgenic Core facility. Healthy blastocysts were implanted into pseudo-pregnant mice. The resulting litters were screened by genomic sequencing to detect the deletion of the *Sprr2a* locus, and mice harboring the deleted allele were bred to homozygosity. *Sprr2a*$^{-/-}$ mice were then backcrossed with wild-type C57BL/6 mice for five generations.

Cell lines and bacterial strains

HT-29 and LS513 cells were obtained from ATCC and were cultured in Dulbecco's Modified Eagle's Medium (DMEM, Thermo Fisher) and Roswell Park Memorial Institute 1640 medium (RPMI 1640, ATCC), respectively. Both media were supplemented with 10%

heat-inactivated fetal bovine serum (FBS) and 10 U/ml Penicillin-Streptomycin (Thermo Fisher). Cells were cultured in the CO_2 incubator at 37°C.

Bacterial strains, including *Enterococcus faecalis, Listeria monocytogenes strain* EGDe, *Escherichia coli* strain K-12, *Bacteroides thetaiotaomicron* strain VPI-5482, and *Citrobacter rodentium* strain DBS100, were obtained from ATCC. *Lactobacillus reuteri* strain 100-23 was a gift from J. Walter (University of Alberta, Canada) (39). *E. faecalis* and *L. monocytogenes* were grown in brain-heart infusion (BHI) broth, *E. coli* and *C. rodentium* were grown in Luria broth (LB), *L. reuteri* was grown in Lactobacilli MRS broth in an anaerobic chamber, and *B. thetaiotaomicron* was grown in tryptone yeast extract glucose (TYG) medium anaerobically.

Antibodies and chemicals

Polyclonal anti-mouse SPRR2A was produced in rabbits by Pacific Immunology (Ramona, CA). The synthesized peptide (CLPSVWPGP) was conjugated to a carrier protein and the conjugate was used to generate the antibody. Other antibodies were purchased from various vendors: anti-human SPRR2A antibody (Abcam, ab125385), anti-MUC2 antibody (Thermo Fisher, MA5-12345), anti-Lysozyme antibody (Santa Cruz, sc-27958), anti-DCLK1 antibody (Abcam, ab202754), anti-GAPDH antibody (Thermo Fisher, PA1-988), anti-β-actin antibody (Cell Signaling, 8457S), anti-β-tubulin (Cell Signaling, 2128S). Fluorescein isothiocyanate (FITC)-conjugated UEA-1 lectin was purchased from GeneTex (GTX01512).

Isolation of intraepithelial lymphocytes (IELs) and lamina propria lymphocytes (LPLs)

Small intestines were dissected from mice, flushed with the ice-cold PBS, and cut open longitudinally. The intestines were cut into small sections that were thoroughly washed with ice-cold PBS. Tissues were incubated at 37°C in Hank's buffered salt solution (HBSS) supplemented with 3% FBS, 1 mM EDTA, and 1 mM DTT. After 30 min, tissues were vortexed for 2 min, and the cell suspensions containing intestinal epithelial cells and the IELs were filtered through a 100-μm cell strainer followed by passage through a glass wool column (Ohio Valley). The cell suspensions were washed and suspended in ice-cold RPMI 1640, and then applied to a 40%:80% Percoll gradient (GE Healthcare). After centrifugation at 800*g* for 20 min, the IELs were collected from the Percoll gradient interface and prepared for RNA isolation and purification.

For LPL isolation, the residual tissue fragments were digested for 1 hour at 37°C in RPMI 1640 containing 0.025 mg/ml Collagenase IV (Sigma-Aldrich), 0.05 mg/ml DNase I (Sigma-Aldrich), and 0.25 units/ml Dispase (BD Biosciences). Cells were filtered through 40-μm cell strainers and applied to a 40%:80% Percoll gradient (GE Healthcare). After centrifugation, the LPL were collected from the gradient interface and prepared for RNA isolation and purification.

Sample collection from human patients

Procedures involving human subjects were approved by the University of Texas Southwestern Medical Center's Institutional Review Board (STU 112010-130). Written

informed consent was obtained from all human participants or legal guardians of participating minors.

Briefly, stool was collected at the time of colonoscopy through direct aspiration of colonic contents. A total of 10 ml was collected per individual. Samples were aliquoted into 1-ml cryovials and immediately frozen in liquid nitrogen. Colonic mucosal tissue samples were collected at time of colonoscopy by standard endoscopic tissue sampling technique. A total of two standard forceps biopsies were obtained per individual. Immediately after collection, samples were placed in RNA*later*™ stabilization solution (Invitrogen) and stored at −80°C. RNA extraction was performed using the QIAGEN RNeasy mini kit on thawed RNA*later* stabilized tissues following the manufacturer's protocol.

Laser capture microdissection and RNA purification

Epithelial cells were captured from mouse small intestines by laser capture microdissection using an Arcturus PixCell IIe system as described (40). Total RNA was isolated from the captured cells using the PicoPure RNA Isolation Kit (Thermo Fisher, KIT0204) following the manufacturer's protocol. RNA from intact tissue or cells was isolated with the RNeasy Plus Universal Mini Kit (Qiagen, 73404) following the manufacturer's protocol.

Quantitative real-time PCR (qPCR) analysis of gene expression

cDNA was synthesized from extracted RNA using M-MLV Reverse Transcriptase (Thermo Fisher, 28025021) following the manufacturer's protocol. qPCR was performed on a QuantStudio 7 Flex RealTime PCR System (Applied Biosystems) as previously described (41). Transcript abundances were normalized to *Gapdh* or 18*S* ribosomal RNA transcript abundance and relative expression values were calculated by the comparative Ct (ΔΔCt) method. Primer sequences are provided in table S3.

In situ hybridization (ISH)

Plasmids containing the entire open reading frame of the mouse *Sprr2a1* gene (NCBI accession: NM_011468.4) with 252 nucleotides were used as templates of RNA probes. Digoxigenin (DIG)-labeled antisense or sense probes were prepared with the HiScribe T7 Quick High Yield RNA Synthesis Kit (NEB, E2050S) following the manufacturer's protocol. The concentrations of riboprobe were determined on a Nanodrop spectrophotometer and the DIG labeling was verified by dot blot using peroxidase-conjugated anti-DIG antibody (Roche, 11207733910).

Paraformaldehyde-fixed paraffin-embedded ileum tissue sections were washed twice in xylene followed by rehydration in decreasing concentrations of ethanol. Tissue sections were permeabilized with 20 μg/ml of proteinase K for 10 min, and treated with ice-cold 20% acetic acid for 20 s. The sections were then pre-hybridized with 50% formamide, 5X saline sodium citrate, 1 mg/ml of yeast tRNA (Roche, 10109517001), 0.1 mg/ml of heparin (Sigma-Aldrich, H3149), 1X Denhardt's solution (Sigma-Aldrich, D2532), and 0.1% Tween-20 at 60°C for 2 hours and hybridized with 0.5 μg/ml riboprobe at 60°C for 16 hours. After washing, sections were incubated with peroxidase-conjugated anti-DIG antibody (Roche, 11207733910), followed by biotin-labeled tyramide (Thermo Fisher, B40951)

for signal amplification. Hybridized probes were detected by ABC-Alkaline phosphatase (Vector Laboratories, AK-5000) and NBT/BCIP (Roche, 11681451001). Images were captured using a Zeiss Axio Imager M1 microscope with Zeiss AxioCam MRm Rev3 and Zeiss EC Plan-Neofluar 10X/0.30 M27 objective lens.

Intestinal organoid culture

Organoids were cultured from small intestinal crypts recovered from 6-8-week-old mice, using a protocol based on previously described methods (33). The protocol was carried out as previously described (42) except that organoid cultures were passaged every 4-7 days.

Immunofluorescence microscopy

For paraffin-embedded sections, mouse intestinal tissues were washed with PBS, fixed in freshly made 4% paraformaldehyde (PFA) at room temperature for 6 hours, and then embedded in paraffin by the UT Southwestern histology core. Sections were washed twice in xylene followed by rehydration in decreasing concentrations of ethanol. Antigen retrieval was performed by boiling in 10 mM sodium citrate for 15 min followed by washing in PBS.

For frozen sections, mouse intestinal tissues or organoids were snap-frozen in optimum cutting temperature (OCT) compound (Fisher, 23-730.571). Ten-micron frozen sections were cut, fixed in 4% PFA at room temperature for 15 min, and washed in PBS. After washing, slides were blocked with 10% FBS, 1% bovine serum albumin (BSA), 1% Trixon X-100 in PBS for 1 hour and incubated with the following primary antibodies at 4°C overnight: anti-mouse SPRR2A at 1:100 dilution, anti-Lysozyme at 1:200 dilution, and FITC-conjugated UEA-1 at 20 μg/ml. Secondary antibodies AlexaFluor ® 488/647 (Thermo Fisher) were diluted 1:400 and applied to slides for 1 hour at room temperature in the dark in a humidified chamber. Slides were washed and mounted with DAPI Fluoromount-G (Southern Biotechnology, 0100-20). Images were captured using a Zeiss Axio Imager M1 microscope with Zeiss AxioCam MRm Rev3 and Zeiss EC Plan-Neofluar 10X/0.30 M27 objective lens.

Fluorescence in situ hybridization (FISH)

Mouse intestinal tissues were cut, directly fixed in Methacarn fixative solution at room temperature for 4 hours, and then embedded in paraffin by the UT Southwestern histology core. Sections were washed twice in xylene followed by rehydration in decreasing concentrations of ethanol. The universal bacterial probe (/5Alex594N/GCTGCCTCCCGTAGGAGT/3AlexF594N/) or the control nonspecific probe (/5Alex594N/ACTCCTACGGGAGGCAGC/3AlexF594N/) were diluted to 100 nM in FISH hybridization buffer (20 mM Tris pH 7.2, 0.9 M NaCl, 0.1% SDS), and applied to slides overnight at 56°C in a humidified chamber. Slides were washed and mounted with DAPI Fluoromount-G (Southern Biotechnology, 0100-20). Images were captured using a Discover Echo Revolve microscope.

Immunoblot

For protein extraction from intestinal tissue and stool samples, samples were added to Lysine Matrix E tubes (MP Biomedicals, 116914050) and then 1 ml of 1X SDS loading buffer

(2% SDS, 10% glycerol, 100 mM DTT, 0.1% bromophenol blue, and 50 mM Tris-HCl pH 6.8) was added. Tubes were then added to a FastPrep-24 5G Homogenizer. After homogenization, the lysates were boiled at 100°C for 10 min and then centrifuged for 10 min at 4°C at 16,100*g*. The supernatants were then transferred to clean tubes.

For protein extraction from cultured cells and intestinal organoids, cells were resuspended in 100 μl RIPA buffer (Thermo Fisher, 89900), and then 100 μl of 2X SDS loading buffer (4% SDS, 20% glycerol, 200 mM DTT, 0.2% bromophenol blue, and 100 mM Tris-HCl pH 6.8) was added. Tubes were boiled at 100°C for 10 min and then centrifuged for 10 min at 4°C at 16,100*g*. The supernatants were then transferred to clean tubes.

The supernatants were separated using a 4 to 20% gradient SDS-PAGE gel (Bio-Rad) then transferred to a PVDF membrane. Membranes were blocked with 5% non-fat milk in TBS-T buffer (0.1% Tween-20 in Tris-buffered saline) then sequentially incubated with primary antibodies and appropriate HRP-conjugated secondary antibodies. Protein bands were detected with ECL reagent (Bio-Rad, 1705060) using a Bio-Rad ChemiDoc™ system.

Recombinant SPRR2A protein expression and purification

Human *SPRR2A* (NCBI accession: NM_005988.3) containing a C-terminal 6xHis tag was cloned into a pFastBac1 vector and heterologously expressed in Sf9 cells (Thermo Fisher). One liter of cells (2.5×10^6 cells/ml) was infected with 10 ml of baculovirus at 28°C. Cells were cultured in suspension at 28°C and were harvested after 48 hours of infection. Harvested cells were resuspended in the buffer containing 25 mM Tris-HCl pH 8.0, 150 mM NaCl, and 1 mM phenylmethylsulfonyl fluoride (PMSF) and lysed by sonication. The mixture was pelleted by centrifugation at 10,000g for 30 min and the supernatant was loaded onto a Ni^{2+} metal affinity column (Qiagen). Non-specific contaminants were washed away with buffer containing 30 mM imidazole and the protein was eluted in buffer containing 300 mM imidazole. The eluate was concentrated in a 3K cutoff Amicon Ultra centrifugal device (Millipore) and further purified by size exclusion chromatography on a Superdex 75™ 10/300 GL column (GE Healthcare Life Sciences) in 10 mM MES pH 5.5 and 25 mM NaCl.

SPRR2A protein was also expressed in *Escherichia coli* BL21-CodonPlus (DE3)-RILP cells (Stratagene) to obtain protein that was free of disulfide bonds. The human *SPRR2A* gene was cloned into the pGEX-6P-1 expression vector (GE Healthcare Life Sciences). The amplicon was placed between the BamHI and XhoI restriction endonuclease sites with an N-terminal GST tag followed by a PreScission protease cleavage site and a C-terminal stop codon. Expression of SPRR2A was induced with 0.4 mM isopropyl-β-D-galactoside (IPTG) for 12 hours at 18°C. Cells were harvested, resuspended in buffer containing 25 mM Tris-HCl pH 8.0 and 150 mM NaCl and lysed by sonication. The mixture was pelleted by centrifugation at 10,000*g* for 30 min and the supernatant was loaded onto the Glutathione Sepharose 4B GST-tagged protein purification resin (GE Healthcare Life Sciences). After four washes with the resuspension buffer, PreScission protease (GE Healthcare Life Sciences) was added to the resin and incubated overnight at 4°C to remove the GST tag. The flow-through, which contained only the untagged SPRR2A protein, was

collected and was further purified by size exclusion chromatography on a Superdex 75™ 10/300 GL column (GE Healthcare Life Sciences) in 10 mM MES pH 5.5 and 25 mM NaCl.

Mass spectrometry

Proteins were analyzed by LC/MS, using a Sciex X500B Q-TOF mass spectrometer coupled to an Agilent 1290 Infinity II HPLC. The protocol was carried out as previously described (43) except for the controller settings: Ion source gas 1 30 psi, ion source gas 2 30 psi, curtain gas 35, CAD gas 7, temperature 300°C, spray voltage 5500 V, declustering potential 125 V, collision energy 10 V. Data were acquired from 400-2000 Da with a 0.5 sec accumulation time.

Bacterial killing assays

Bacterial killing assays were performed as previously described (21, 23). Briefly, 10-ml bacterial cultures were grown to midlogarithmic phase and then pelleted and washed in 10 ml of standard assay buffer (10 mM MES pH 5.5 and 25 mM NaCl). Purified SPRR2A proteins were added in varying concentrations (0-10 μM) to ~5×10^6 CFU/ml bacteria. Bacteria were incubated at 37°C for 2 hours, plated onto appropriate agar plates at various dilutions, and incubated overnight at 37°C. Surviving colonies were counted and calculated as a percentage of the remaining colonies in the buffer only sample.

Bacterial binding assays

Bacterial cultures (10 ml) were grown to mid-logarithmic phase. Cells were pelleted, washed and resuspended in 1 ml of 90% ethanol. Bacteria were fixed for 20 min at room temperature, then pelleted and washed twice in PBS. The cells were resuspended in standard assay buffer (10 mM MES pH 5.5 and 25 mM NaCl), and 10 μM purified SPRR2A was added to ~5×10^8 CFU/ml bacteria with a total volume of 200 μl. After a 10-min incubation at room temperature, 20 μl of each sample was collected as input (I). Samples were then centrifuged at 4°C for 10 min at 8000*g*. The supernatants (S) were collected to examine proteins that were not bound to bacteria. The pellets (P), which contained the bound protein, were washed twice with 200 μl of standard assay buffer by recentrifugation and then resuspended in 180 μl of buffer. The I, S, and P fractions were analyzed by SDS-PAGE and Coomassie blue staining.

Propidium iodide (PI) uptake assay

Propidium iodide (PI) uptake assays were performed as previously described (23, 41). Briefly, bacterial cultures were grown to midlogarithmic phase and then pelleted and washed in standard assay buffer (10 mM MES pH 5.5 and 25 mM NaCl). Bacteria were then diluted into standard assay buffer (~5×10^8 cells/ml) containing 5.5 μg/ml of PI (Thermo Fisher, P3566). Bacterial samples (90 μl each) were added to black 96-well Costar plates (Fisher, 07-200-567) and placed into a Spectramax plate reader (Molecular Devices) that was preequilibrated to 37°C. After an initial reading, 10 μl of recombinant purified SPRR2A proteins at varying concentrations or BSA were added and fluorescence outputs (excitation, 535 nm; emission, 617 nm) were measured every 5 min for 1 hour. Bacterial

permeabilization activity was measured against the maximum fluorescence output from the positive control (0.05% SDS).

Lipid strip assay

Membrane lipid strips (Echelon, P-6002) were used following the manufacturer's protocol. Briefly, the lipid strips were blocked with blocking buffer (10 mM MES pH 5.5, 25 mM NaCl, 2% BSA, and 0.05% Tween-20) for 1 hour at room temperature. Recombinant purified SPRR2A proteins were diluted to 1 μg/ml in blocking buffer and incubated with the lipid strip overnight at 4°C. After washing three times with washing buffer (10 mM MES pH 5.5, 25 mM NaCl, and 0.05% Tween-20), the lipid strip was sequentially incubated with anti-SPRR2A antibody and HRP-conjugated secondary antibody. Protein dots were detected with ECL reagent (Bio-Rad, 1705060) using a Bio-Rad ChemiDoc™ system.

Liposome preparation

Unilamellar liposomes were prepared using lipids from Avanti Polar Lipids: 1-palmitoyl-2-oleoyl-sn-glycero-3-phosphocholine (PC) (850457C), 1,2-dioleoyl-sn-glycero-3-phospho-L-serine (PS) (840035C), 1,3-bis[1,2-dimyristoyl-sn-glycero-3-phospho]-glycerol, or cardiolipin (710332C). The lipids were prepared as previously described (23, 27). Lipids dissolved in chloroform were mixed in defined molar ratios in glass tubes and then dried under a stream of N_2, followed by drying under vacuum overnight to ensure complete removal of organic solvents. Dried lipids were resuspended in standard assay buffer (10 mM MES pH 5.5, 25 mM NaCl), or standard assay buffer containing 5(6)-carboxyfluorescein (CF) (Sigma, 21877) or fluorescein-dextran 10 (FD10) (Thermo Fish, D1821). Lipids were transferred to a 2-ml freezing vial, subjected to five freeze-thaw cycles in liquid N_2, and stored at −80°C. Lipids were then thawed and passed through a 100 nm pore membrane using a mini-extruder kit (Avanti Polar Lipids, 610000). Dye-free or CF-loaded liposomes were purified on a PD-10 column (GE Healthcare Life Sciences), and liposomes loaded with FD10 were purified by size-exclusion chromatography on a Superdex 200 Increase 10/300 GL column (GE Healthcare Life Sciences).

Liposome binding assay

Recombinant purified SPRR2A (5 μM) was incubated with liposomes (500 μM lipids) at room temperature for 30 min in a total volume of 200 μl. Twenty-microliter samples were collected as input (I). Samples were then centrifuged in a Beckman Optima XE-90 ultracentrifuge at 4°C for 30 min at 100,000*g*. The supernatant (S) was collected to examine proteins not bound to the liposome. The pellets (P), which contained the bound protein, were washed twice with 200 μl of buffer by recentrifugation and then resuspended to 180 μl. The I, S, and P fractions were analyzed by SDS-PAGE and Coomassie blue staining.

Liposome leakage assay

Prepared CF or FD-10 loaded liposomes were diluted in standard assay buffer (10 mM MES pH 5.5 and 25 mM NaCl) to a final concentration of 1 mM. A QuantaMaster 300 fluorometer (Photon Technology International) was used to monitor fluorescence (excitation, 490 nm; emission, 516 nm). One hundred microliters of liposomes was used each time.

After allowing establishment of a stable baseline for 200 s, 10 μl of recombinant purified SPRR2A proteins at varying concentrations was added, and the fluorescence was monitored for another 800 s. At the end time point, 10 μl of 10% n-octyl glucoside (OG) (Anatrace, O311) was added to completely disrupt the liposomes. Fluorescence was measured over time in seconds and is expressed as a percentage of total dye release by the detergent OG.

Electron microscopy

For electron microscopy of bacteria, 10-ml bacterial cultures (*Listeria monocytogenes* or *Enterococcus faecalis*) were grown to midlogarithmic phase and then pelleted and washed in 10 ml of standard assay buffer (10 mM MES pH 5.5 and 25 mM NaCl). Bacteria were resuspended in 1 ml of standard assay buffer. Purified SPRR2A was added at a final concentration of 10 μM to 300 μl of resuspended bacteria and incubated at 37°C for 2 hours. Bacteria were then centrifuged for 10 min at 16,100*g*, resuspended in cross-linking reagent (4% paraformaldehyde and 5% glutaraldehyde in 0.1 M sodium phosphate buffer, pH 7.4), and incubated overnight at 4°C. After washing three times with the same buffer, bacterial pellets were embedded in 3% agarose, sliced into blocks (1 mm^3), and fixed with 1% osmium tetroxide and 0.8% potassium ferricyanide in 0.1 M sodium phosphate buffer for 1.5 hours at room temperature. The cells were then stained with 1% aqueous uranyl acetate for 1 hour. Cells were dehydrated stepwise through increasing ethanol concentrations and then transitioned into propylene oxide. The cells were permeated with Embed-812 resin, and polymerized at 60°C overnight. Blocks were sectioned on a Leica Ultracut 7 ultramicrotome (Leica Microsystems) using a diamond knife (Diatome). The sections were then deposited onto copper grids and stained with 2% aqueous uranyl acetate and lead citrate. Images were captured on a Tecnai G2 spirit transmission electron microscope (Thermo Fisher) using a LaB6 source at 120 kV.

For electron microscopy of liposomes, recombinant purified SPRR2A (5 μM) was incubated with liposomes (500 μM lipids) at room temperature for 30 min. Aliquots of the mixture (5 μl were transferred to carbon support films on electron microscopy grids (Electron Microscopy Sciences, FCF200-CU) and negatively stained with 2% uranyl acetate. Images were acquired on a Tecnai G2 Spirit transmission electron microscope (Thermo Fisher).

DNA extraction for 16*S* rRNA analysis

For isolation of small intestinal lumenal contents, a 2-cm section of ileum was cut and lumenal contents were flushed with 2 ml of ice-cold PBS into a pre-weighed 2-ml sterile freezing vial. The contents were pelleted at 16,100*g* for 10 min, the supernatants removed, and the pellets weighed prior to further processing. For isolation of lumenal contents from the colon, a section of mid-colon was cut open longitudinally. Whole fecal pellets were extracted and weighed. For analysis of tissue-associated bacteria, the same tissue samples that were used for analysis of lumenal contents were cut open longitudinally and washed in ice cold PBS until visibly clean. The whole tissue was then weighed prior to further processing.

For DNA extraction from isolated lumenal contents, DNA was extracted and purified using the FastDNA Spin Kit (MP Biomedicals 116560-200) following the manufacturer's

protocol. For DNA extraction from tissue-associated bacteria, samples were added to Lysine Matrix E tubes (MP Biomedicals #116914050) and then 1 ml of lysis buffer (1X Tris-EDTA buffer, 0.5% SDS, and 200 μg/ml of proteinase K) was added. Tubes were incubated at 55°C for 1 hour, then added to a FastPrep-24 5G homogenizer. After homogenization, the lysates were centrifuged for 10 min at 4°C at 16,100*g*. The supernatants were then transferred to clean tubes, and DNA was extracted with 750 μl phenol:chloroform. The upper layer containing the DNA was precipitated with sodium acetate and ethanol and stored in TE buffer at −80°C.

16*S* qPCR analysis

16*S* qPCR analysis was performed as previously described (22, 23). Briefly, to allow quantification of low-copy number bacterial 16*S* DNA by qPCR, limited cycle number (LCN) PCRs were used to amplify the entire 16*S* gene. Twenty microliters of LCN PCRs was prepared using the HotStarTaq polymerase kit (Qiagen), 0.2 μM universal forward primer 27F (5′-AGAGTTTGATCMTGGCTCAG-3′) and reverse primer 1492R (5′-CGGTTACCTTGTTACGACTT-3′), and 500 ng of template DNA. After 16 thermocycles, the PCR products were diluted 1:10 into H_2O, and the diluted DNA samples were analyzed by qPCR using the SYBR Green kit (Thermo Fisher, 4309155) with taxon-specific primers (listed in table S3). PCR control reactions containing water were included to identify possible contamination. The 16*S* data were initially normalized to data from the water control and then normalized to the lumenal content or tissue weight. The total number of 16*S* copies was determined using standard curves generated from quantified standard plasmids.

16*S* rRNA sequencing and data analysis

The hypervariable regions V3 and V4 of the bacterial 16*S* rRNA gene were sequenced and analyzed as previously described (41). 16*S* rRNA gene sequencing data are available from the Sequence Read Archive (SRA) with project ID PRJNA743545.

Conventionalization of germ-free mice and LPS challenge

For conventionalization, ~50 mg of feces was collected from a conventional wild-type mouse and suspended in 1 ml of PBS. Fecal debris was pelleted and 200 μl of the supernatant was used for oral gavage of each germ-free mouse. Mice were raised for 7 more days in contact with cage bedding collected from the SPF barrier facility at the University of Texas Southwestern Medical Center. For LPS challenge, 8-10-week-old germ-free Swiss-Webster mice were given 500 μg of γ-irradiated LPS (Sigma-Aldrich, L4391) every 12 hours for 3 days through oral gavage. Mice were sacrificed 12 hours after the last treatment.

Antibiotic treatment of mice

Conventionally raised mice were administered 200 μl of antibiotic cocktail water containing 2 mg/ml of neomycin, 2 mg/ml of gentamycin, 2 mg/ml of metronidazole, 2 mg/ml of streptomycin, and 1 mg/ml of vancomycin through oral gavage. Mice were raised for 7 more days using the drinking water containing 1 mg/ml of neomycin, 1 mg/ml of gentamycin,

1 mg/ml of metronidazole, 1 mg/ml of streptomycin, 0.5 mg/ml of vancomycin, and 10% sucrose. Microbiota depletion was verified by aerobic and anaerobic culture of fecal pellets.

Intestinal permeability assay

Intestinal permeability assays were performed by treating mice with fluorescein isothiocyanate-dextran (FITC-dextran) (Sigma-Aldrich, FD4-1G) through oral gavage, which is normally too large to pass across the intestinal barrier. However, when there is intestinal damage, paracellular permeability is increased, and FITC-dextran penetrates into gut tissue and appears in serum. Indomethacin (Sigma-Aldrich, I7378), a non-steroidal anti-inflammatory drug (NSAID) that can induce intestinal damage in mice, was used as a positive control.

For the experimental group, wild-type and *Sprr2a*$^{-/-}$ mice were treated with 190 μl of 7% DMSO in PBS by oral gavage. For the positive control group, mice were treated with 190 μl of indomethacin (1.5 mg/ml in 7% DMSO in PBS) by oral gavage. After 1 hour, mice in both groups were treated with 190 μl of FITC-dextran (80 mg/ml in PBS) by oral gavage. Mice were sacrificed 4 hours later and sera were collected. The sera were then centrifuged for 20 min at 4°C at 1740*g* and the supernatants were collected. Serum FITC-dextran levels were measured by fluorescence microplate assay against a FITC-dextran standard curve using a Spectramax plate reader (Molecular Devices).

Listeria monocytogenes infection

Listeria monocytogenes strain EGDe (erythromycin-resistant) was grown overnight in brain-heart infusion (BHI) broth containing 20 μg/ml erythromycin at 37°C. Wild-type and *Sprr2a*$^{-/-}$ mice were treated with erythromycin (0.4 mg per mice) by oral gavage the day before infection. Mice were inoculated with 1.0×10^9 *Listeria monocytogenes* for tissue dissemination experiments or 2.5×10^9 bacteria for survival experiments by oral gavage. For tissue dissemination experiments, mice were sacrificed 1 day after infection, and the mesenteric lymph nodes (MLN), liver, and spleen were collected and weighed. Tissues were homogenized in ice-cold PBS and the numbers of *Listeria monocytogenes* were counted by dilution plating on BHI-erythromycin agar plates. We calculated the limit of detection as [CFU (minimum)] × [dilution factor] / [tissue weight]. Data points below the limit of detection indicate that no *L. monocytogenes* colonies grew on any of the three replicate plates.

Recombinant IL-13 and IL-22 treatment

Wild-type BALB/c mice were injected intraperitoneally with 1.5 μg of carrier-free recombinant mouse IL-13 (BioLegend, 575906) or IL-22 (BioLegend, 576206) every other day for a total of four treatments. Mice were sacrificed on the day after the last injection.

Heligmosomoides polygyrus infection

Heligmosomoides polygyrus (*H. polygyrus*; recently renamed *H. bakeri* (44)) stocks were propagated as previously described (45, 46) with a few exceptions. Briefly, B6.129S2(C)-*Stat6*^{tm1Gru} (Jackson stock, 005977) (38) or wild-type C57BL/6 mice housed in a BSL2 animal facility were infected with 400 *H. polygyrus* L3 larvae by oral gavage. On day 13 of

infection, grates were placed in the cages and feces were collected for the next 3 days. Feces were mashed and mixed with activated, washed charcoal (Sigma-Aldrich, C2764-500G), then plated on Whatman filter paper in petri dishes. PBS was added to the dishes until a pool formed around the filter paper. After 7-10 days of incubation in a humid box, the L3 larvae were collected with a modified Baermann apparatus filled with warm PBS. The tube of the Baermann apparatus was plugged with a stopper. A metal grate was placed at the top of the funnel, then one layer of muslin and one layer of Kimwipe (Fisher Scientific) were placed on top of that. The fecal mixture was spread on top of both layers, and the larvae were allowed to fall for 2 hours. The PBS from the apparatus was collected into a beaker and the larvae were concentrated by centrifugation at 300g for 10 min with no brake. After the larvae were concentrated, they were put through the Baermann apparatus and then concentrated by centrifugation a second time. The larvae were washed three times with PBS and stored at 4°C in PBS. A new stock was generated every 6 months.

For *H. polygyrus* infection experiments, wild-type, *Stat6*$^{-/-}$ and *Sprr2a*$^{-/-}$ mice were inoculated with 200 L3 *H. polygyrus* larvae through oral gavage in the BSL2 animal facility. After 2 weeks, mice were sacrificed, and the intestinal tissues were collected for further studies.

H. polygyrus worm and egg counting

To quantify worm burden, small intestines and their lumenal contents were collected and placed in 10 ml of PBS in Petri dishes at room temperature. The intestines were dissected longitudinally and worms associated with the intestinal tissue were collected by scraping with forceps. After 1 hour of incubation at 37°C, worms were counted manually using forceps.

For egg counting, 1-2 fecal pellets were collected and weighed. Three milliliters of water was added to the fecal pellets in 15-ml conical tubes and vortexed periodically until the pellets were completely dispersed. Just before each sample was added to the McMaster egg counter (Electron Microscopy Sciences, 63512-75), an equal volume of supersaturated NaCl solution was added to the tube. Eggs were counted under a microscope, and two independent counts were averaged. Egg numbers were normalized to the weight of fecal pellets.

Statistics

We used two-tailed Student's *t*-tests to determine the statistical significance of a difference between two treatments when a parametric test was appropriate. We used the Mann–Whitney *U* test for experiments requiring a non-parametric statistical test (e.g., Fig. 3E). For data having unequal variances among different experimental groups and following a lognormal distribution, a logarithmic transform was performed before the statistical analysis. The log-rank test was used in survival experiments where the null hypothesis was that there is no difference between experimental groups in the probability of lethal morbidity at any time point. Statistical details of experiments are provided in the figure legends, including how significance was defined and the statistical methods used. Data represent mean ± standard error of the mean (SEM). All statistical analyses were performed

with GraphPad Prism software. For all tests, *P*-values lower than 0.05 were considered statistically significant.

Supplementary Material

Refer to Web version on PubMed Central for supplementary material.

ACKNOWLEDGEMENTS

We thank Dr. X. Zhan for advice on the generation of *Sprr2a*$^{-/-}$ mice; M. Spence and N. Salinas for assistance with mouse experiments; P. Doss, R. Roman, R. Jackson, and Dr. A. Darehshouri (UT Southwestern Electron Microscopy Core) for assistance with electron microscopy; Dr. A. Lemoff (UT Southwestern Proteomics Core) for assistance with mass spectrometry; Dr. B. Evers (UT Southwestern Histopathology Core) for assistance with mouse histology analysis; and Dr. E. Burstein for collaboration on patient sample collection.

Funding:

This work was supported by NIH grants R01 DK070855 (L.V.H.), R01 AI130020 (T.A.R.), and K99 DK120897 (Z.K.); Welch Foundation Grant I-1874 (L.V.H.); American Heart Association Grant 17SDG33670071 (T.A.R.); Cancer Prevention and Research Institute of Texas Grant RP200118 (T.A.R.); the Pew Charitable Trusts (T.A.R.); the Walter M. and Helen D. Bader Center for Research on Arthritis and Autoimmune Diseases (L.V.H.); and the Howard Hughes Medical Institute (L.V.H.). C.M.Z., Z.K., and M.P. were supported by NIH T32 AI005284.

Data and materials availability:

16*S* rRNA gene sequencing data are available from the Sequence Read Archive (SRA) with project ID PRJNA743545. All other data are available in the main text or the supplementary materials.

REFERENCES AND NOTES

1. Clemente JC, Ursell LK, Parfrey LW, Knight R, The impact of the gut microbiota on human health: an integrative view. Cell 148, 1258–1270 (2012). [PubMed: 22424233]
2. Rapin A, Harris NL, Helminth-bacterial interactions: cause and consequence. Trends Immunol 39, 724–733 (2018). [PubMed: 29941203]
3. Coakley G, Harris NL, The intestinal epithelium at the forefront of host-helminth interactions. Trends Parasitol 36, 761–772 (2020). [PubMed: 32713764]
4. Gallo RL, Hooper LV, Epithelial antimicrobial defence of the skin and intestine. Nat Rev Immunol 12, 503–516 (2012). [PubMed: 22728527]
5. Mukherjee S, Hooper LV, Antimicrobial defense of the intestine. Immunity 42, 28–39 (2015). [PubMed: 25607457]
6. Maizels RM, Yazdanbakhsh M, Immune regulation by helminth parasites: cellular and molecular mechanisms. Nat Rev Immunol 3, 733–744 (2003). [PubMed: 12949497]
7. Allen JE, Maizels RM, Diversity and dialogue in immunity to helminths. Nat Rev Immunol 11, 375–388 (2011). [PubMed: 21610741]
8. Gause WC, Wynn TA, Allen JE, Type 2 immunity and wound healing: evolutionary refinement of adaptive immunity by helminths. Nat Rev Immunol 13, 607–614 (2013). [PubMed: 23827958]
9. Sorobetea D, Svensson-Frej M, Grencis R, Immunity to gastrointestinal nematode infections. Mucosal Immunol 11, 304–315 (2018). [PubMed: 29297502]
10. Hooper LV, Wong MH, Thelin A, Hansson L, Falk PG, Gordon JI, Molecular analysis of commensal host-microbial relationships in the intestine. Science 291, 881–884 (2001). [PubMed: 11157169]

11. Gibbs S, Fijneman R, Wiegant J, van Kessel AG, van De Putte P, Backendorf C, Molecular characterization and evolution of the SPRR family of keratinocyte differentiation markers encoding small proline-rich proteins. Genomics 16, 630–637 (1993). [PubMed: 8325635]
12. Mueller A, O'Rourke J, Grimm J, Guillemin K, Dixon MF, Lee A, Falkow S, Distinct gene expression profiles characterize the histopathological stages of disease in Helicobacter-induced mucosa-associated lymphoid tissue lymphoma. Proc Natl Acad Sci U S A 100, 1292–1297 (2003). [PubMed: 12552104]
13. Sun FJ, Kaur S, Ziemer D, Banerjee S, Samuelson LC, De Lisle RC, Decreased gastric bacterial killing and up-regulation of protective genes in small intestine in gastrin-deficient mouse. Dig Dis Sci 48, 976–985 (2003). [PubMed: 12772799]
14. Domachowske JB, Bonville CA, Easton AJ, Rosenberg HF, Differential expression of proinflammatory cytokine genes in vivo in response to pathogenic and nonpathogenic pneumovirus infections. J Infect Dis 186, 8–14 (2002). [PubMed: 12089656]
15. Vos JB, Datson NA, van Kampen AH, Luyf AC, Verhoosel RM, Zeeuwen PL, Olthuis D, Rabe KF, Schalkwijk J, Hiemstra PS, A molecular signature of epithelial host defense: comparative gene expression analysis of cultured bronchial epithelial cells and keratinocytes. BMC Genomics 7, 9 (2006). [PubMed: 16420688]
16. Tamoutounour S, Han SJ, Deckers J, Constantinides MG, Hurabielle C, Harrison OJ, Bouladoux N, Linehan JL, Link VM, Vujkovic-Cvijin I, Perez-Chaparro PJ, Rosshart SP, Rehermann B, Lazarevic V, Belkaid Y, Keratinocyte-intrinsic MHCII expression controls microbiota-induced Th1 cell responses. Proc Natl Acad Sci U S A 116, 23643–23652 (2019). [PubMed: 31672911]
17. Candi E, Schmidt R, Melino G, The cornified envelope: a model of cell death in the skin. Nat Rev Mol Cell Biol 6, 328–340 (2005). [PubMed: 15803139]
18. Haber AL, Biton M, Rogel N, Herbst RH, Shekhar K, Smillie C, Burgin G, Delorey TM, Howitt MR, Katz Y, Tirosh I, Beyaz S, Dionne D, Zhang M, Raychowdhury R, Garrett WS, Rozenblatt-Rosen O, Shi HN, Yilmaz O, Xavier RJ, Regev A, A single-cell survey of the small intestinal epithelium. Nature 551, 333–339 (2017). [PubMed: 29144463]
19. Ghandi M, Huang FW, Jane-Valbuena J, Kryukov GV, Lo CC, McDonald ER 3rd, Barretina J, Gelfand ET, Bielski CM, Li H, Hu K, Andreev-Drakhlin AY, Kim J, Hess JM, Haas BJ, Aguet F, Weir BA, Rothberg MV, Paolella BR, Lawrence MS, Akbani R, Lu Y, Tiv HL, Gokhale PC, de Weck A, Mansour AA, Oh C, Shih J, Hadi K, Rosen Y, Bistline J, Venkatesan K, Reddy A, Sonkin D, Liu M, Lehar J, Korn JM, Porter DA, Jones MD, Golji J, Caponigro G, Taylor JE, Dunning CM, Creech AL, Warren AC, McFarland JM, Zamanighomi M, Kauffmann A, Stransky N, Imielinski M, Maruvka YE, Cherniack AD, Tsherniak A, Vazquez F, Jaffe JD, Lane AA, Weinstock DM, Johannessen CM, Morrissey MP, Stegmeier F, Schlegel R, Hahn WC, Getz G, Mills GB, Boehm JS, Golub TR, Garraway A, Sellers WR, Next-generation characterization of the Cancer Cell Line Encyclopedia. Nature 569, 503–508 (2019). [PubMed: 31068700]
20. Hooper LV, Stappenbeck TS, Hong CV, Gordon JI, Angiogenins: a new class of microbicidal proteins involved in innate immunity. Nat Immunol 4, 269–273 (2003). [PubMed: 12548285]
21. Cash HL, Whitham CV, Behrendt CL, Hooper LV, Symbiotic bacteria direct expression of an intestinal bactericidal lectin. Science 313, 1126–1130 (2006). [PubMed: 16931762]
22. Vaishnava S, Yamamoto M, Severson KM, Ruhn KA, Yu X, Koren O, Ley R, Wakeland EK, Hooper LV, The antibacterial lectin RegIIIγ promotes the spatial segregation of microbiota and host in the intestine. Science 334, 255–258 (2011). [PubMed: 21998396]
23. Propheter DC, Chara AL, Harris TA, Ruhn KA, Hooper LV, Resistin-like molecule β is a bactericidal protein that promotes spatial segregation of the microbiota and the colonic epithelium. Proc Natl Acad Sci U S A 114, 11027–11033 (2017). [PubMed: 28973871]
24. Zasloff M, Antimicrobial peptides of multicellular organisms. Nature 415, 389–395 (2002). [PubMed: 11807545]
25. Malik E, Dennison SR, Harris F, Phoenix DA, pH dependent antimicrobial peptides and proteins, their mechanisms of action and potential as therapeutic agents. Pharmaceuticals (Basel) 9, (2016).
26. Pelaseyed T, Bergstrom JH, Gustafsson JK, Ermund A, Birchenough GM, Schutte A, van der Post S, Svensson F, Rodriguez-Pineiro AM, Nystrom EE, Wising C, Johansson ME, Hansson GC, The mucus and mucins of the goblet cells and enterocytes provide the first defense line of

the gastrointestinal tract and interact with the immune system. Immunol Rev 260, 8–20 (2014). [PubMed: 24942678]

27. Mukherjee S, Zheng H, Derebe MG, Callenberg KM, Partch CL, Rollins D, Propheter DC, Rizo J, Grabe M, Jiang QX, Hooper LV, Antibacterial membrane attack by a pore-forming intestinal C-type lectin. Nature 505, 103–107 (2014). [PubMed: 24256734]
28. Li SC, Goto NK, Williams KA, Deber CM, Alpha-helical, but not beta-sheet, propensity of proline is determined by peptide environment. Proc Natl Acad Sci U S A 93, 6676–6681 (1996). [PubMed: 8692877]
29. Johansson ME, Phillipson M, Petersson J, Velcich A, Holm L, Hansson GC, The inner of the two Muc2 mucin-dependent mucus layers in colon is devoid of bacteria. Proc Natl Acad Sci U S A 105, 15064–15069 (2008). [PubMed: 18806221]
30. Knight PA, Pemberton AD, Robertson KA, Roy DJ, Wright SH, Miller HR, Expression profiling reveals novel innate and inflammatory responses in the jejunal epithelial compartment during infection with Trichinella spiralis. Infect Immun 72, 6076–6086 (2004). [PubMed: 15385512]
31. Voehringer D, Stanley SA, Cox JS, Completo GC, Lowary TL, Locksley RM, Nippostrongylus brasiliensis: identification of intelectin-1 and -2 as Stat6-dependent genes expressed in lung and intestine during infection. Exp Parasitol 116, 458–466 (2007). [PubMed: 17420014]
32. Entwistle LJ, Pelly VS, Coomes SM, Kannan Y, Perez-Lloret J, Czieso S, Silva Dos Santos M, MacRae JI, Collinson L, Sesay A, Nikolov N, Metidji A, Helmby H, Hui DY, Wilson MS, Epithelial-cell-derived phospholipase A2 group 1B Is an endogenous anthelmintic. Cell Host Microbe 22, 484–493 e485 (2017). [PubMed: 29024642]
33. Sato T, van Es JH, Snippert HJ, Stange DE, Vries RG, van den Born M, Barker N, Shroyer NF, van de Wetering M, Clevers H, Paneth cells constitute the niche for Lgr5 stem cells in intestinal crypts. Nature 469, 415–418 (2011). [PubMed: 21113151]
34. Scocchi M, Tossi A, Gennaro R, Proline-rich antimicrobial peptides: converging to a non-lytic mechanism of action. Cell Mol Life Sci 68, 2317–2330 (2011). [PubMed: 21594684]
35. Artis D, Wang ML, Keilbaugh SA, He W, Brenes M, Swain GP, Knight PA, Donaldson DD, Lazar MA, Miller HRP, Schad GA, Scott P, Wu GD, RELMbeta/FIZZ2 is a goblet cell-specific immune-effector molecule in the gastrointestinal tract. Proc Natl Acad Sci U S A 101, 13596–13600 (2004). [PubMed: 15340149]
36. Ramanan D, Bowcutt R, Lee SC, Tang MS, Kurtz ZD, Ding Y, Honda K, Gause WC, Blaser MJ, Bonneau RA, Lim YA, Loke P, Cadwell K, Helminth infection promotes colonization resistance via type 2 immunity. Science 352, 608–612 (2016). [PubMed: 27080105]
37. Adachi O, Kawai T, Takeda K, Matsumoto M, Tsutsui H, Sakagami M, Nakanishi K, Akira S, Targeted disruption of the MyD88 gene results in loss of IL-1- and IL-18-mediated function. Immunity 9, 143–150 (1998). [PubMed: 9697844]
38. Kaplan MH, Schindler U, Smiley ST, Grusby MJ, Stat6 is required for mediating responses to IL-4 and for development of Th2 cells. Immunity 4, 313–319 (1996). [PubMed: 8624821]
39. Frese SA, Benson AK, Tannock GW, Loach DM, Kim J, Zhang M, Oh PL, Heng NC, Patil PB, Juge N, Mackenzie DA, Pearson BM, Lapidus A, Dalin E, Tice H, Goltsman E, Land M, Hauser L, Ivanova N, Kyrpides NC, Walter J, The evolution of host specialization in the vertebrate gut symbiont Lactobacillus reuteri. PLoS Genet 7, e1001314 (2011). [PubMed: 21379339]
40. Stappenbeck TS, Hooper LV, Manchester JK, Wong MH, Gordon JI, Laser capture microdissection of mouse intestine: characterizing mRNA and protein expression, and profiling intermediary metabolism in specified cell populations. Methods Enzymol 356, 167–196 (2002). [PubMed: 12418197]
41. Harris TA, Gattu S, Propheter DC, Kuang Z, Bel S, Ruhn KA, Chara AL, Edwards M, Zhang C, Jo JH, Raj P, Zouboulis CC, Kong HH, Segre JA, Hooper LV, Resistin-like molecule α provides vitamin-A-dependent antimicrobial protection in the skin. Cell Host Microbe 777–788 (2019). [PubMed: 31101494]
42. Wang Y, Kuang Z, Yu X, Ruhn KA, Kubo M, Hooper LV, The intestinal microbiota regulates body composition through NFIL3 and the circadian clock. Science 357, 912–916 (2017). [PubMed: 28860383]

43. Black MH, Osinski A, Gradowski M, Servage KA, Pawlowski K, Tomchick DR, Tagliabracci VS, Bacterial pseudokinase catalyzes protein polyglutamylation to inhibit the SidE-family ubiquitin ligases. Science 364, 787–792 (2019). [PubMed: 31123136]

44. Behnke J, Harris PD, *Heligmosomoides bakeri*: a new name for an old worm? Trends Parasitol 524–529 (2010). [PubMed: 20729145]

45. Camberis M, Le Gros G, Urban J Jr., Animal model of Nippostrongylus brasiliensis and Heligmosomoides polygyrus. Curr Protoc Immunol Chapter 19, Unit 19 12 (2003).

46. Johnston CJ, Robertson E, Harcus Y, Grainger JR, Coakley G, Smyth DJ, McSorley HJ, Maizels R, Cultivation of Heligmosomoides polygyrus: an immunomodulatory nematode parasite and its secreted products. J Vis Exp, e52412 (2015). [PubMed: 25867600]

47. Kuang Z, Wang Y, Li Y, Ye C, Ruhn KA, Behrendt CL, Olson EN, Hooper LV, The intestinal microbiota programs diurnal rhythms in host metabolism through histone deacetylase 3. Science 365, 1428–1434 (2019). [PubMed: 31604271]

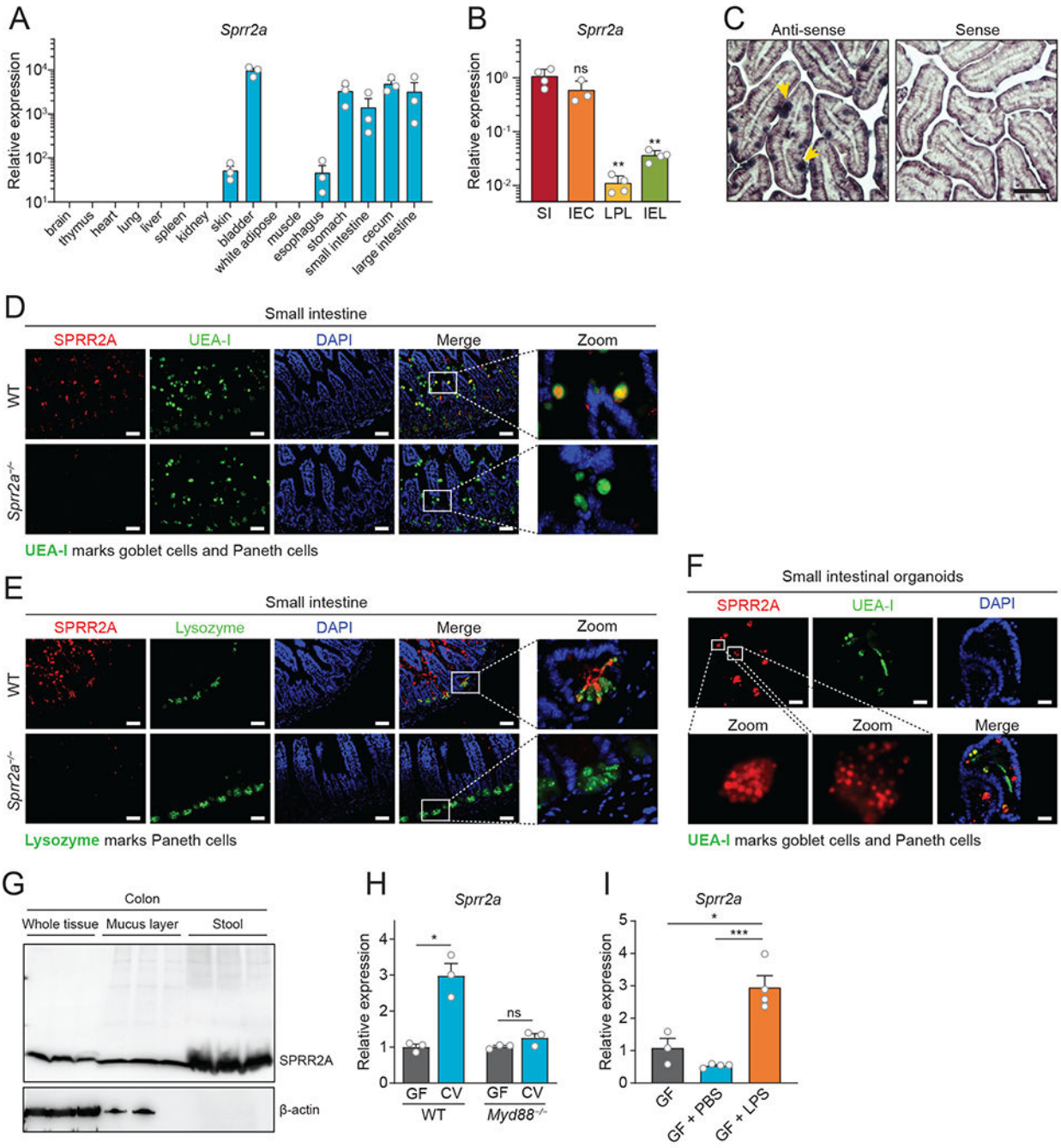

Fig. 1. SPRR2A is expressed in goblet cells and Paneth cells in the mouse intestine.

(A) Quantitative PCR (qPCR) analysis of *Sprr2a* expression in various organs of wild-type C57BL/6 mice. Values were normalized to 18*S* rRNA expression. n=3 mice per group. **(B)** qPCR analysis of *Sprr2a* expression in mouse small intestine (SI), small intestinal epithelial cells (IEC) acquired by laser capture microdissection, lamina propria lymphocytes (LPL), and intraepithelial lymphocytes (IEL). Values were normalized to 18*S* rRNA expression. **(C)** In situ hybridization of small intestine sections with anti-sense and sense *Sprr2a* RNA probes. Examples of positive signals are indicated by yellow arrowheads. Scale bar=50 μm.

(**D** and **E**) Immunofluorescence detection of SPRR2A (red) in sections of paraffin-embedded mouse small intestine. *Ulex europaeus* agglutinin-I (UEA-I) (D) and anti-lysozyme antibody (E) were used to identify goblet cells (UEA-I) and Paneth cells (UEA-I and anti-lysozyme). Nuclei were detected with 4',6-diamidino-2-phenylindole (DAPI). Sections from *Sprr2a*$^{-/-}$ mice (generated as shown in fig. S2) were used as negative controls. Scale bars=50 μm. **(F)** Immunofluorescence detection of SPRR2A (red) in OCT-embedded frozen sections of mouse small-intestinal organoids. Scale bars=25 μm. **(G)** Immunoblot detection of SPRR2A protein in mouse colon, the colon mucus layer, and stool samples. (**H**) qPCR analysis of epithelial cell *Sprr2a* expression in germ-free (GF) wild-type (WT) and *Myd88*-deficient (*Myd88*$^{-/-}$) C57BL/6 mice with or without conventionalization (CV). Epithelial cells were harvested by laser capture microdissection. Values were normalized to *Gapdh* expression. n=3 mice per group. (**I**) qPCR analysis of *Sprr2a* expression in the small intestines of germ-free Swiss-Webster mice treated with lipopolysaccharide (LPS). PBS was administered as a vehicle control. Values were normalized to *Gapdh* expression. n=3-4 mice per group. Means ± SEM (error bars) are plotted. *P<0.05; **P<0.01; ***P<0.001; ns, not significant by two-tailed t test.

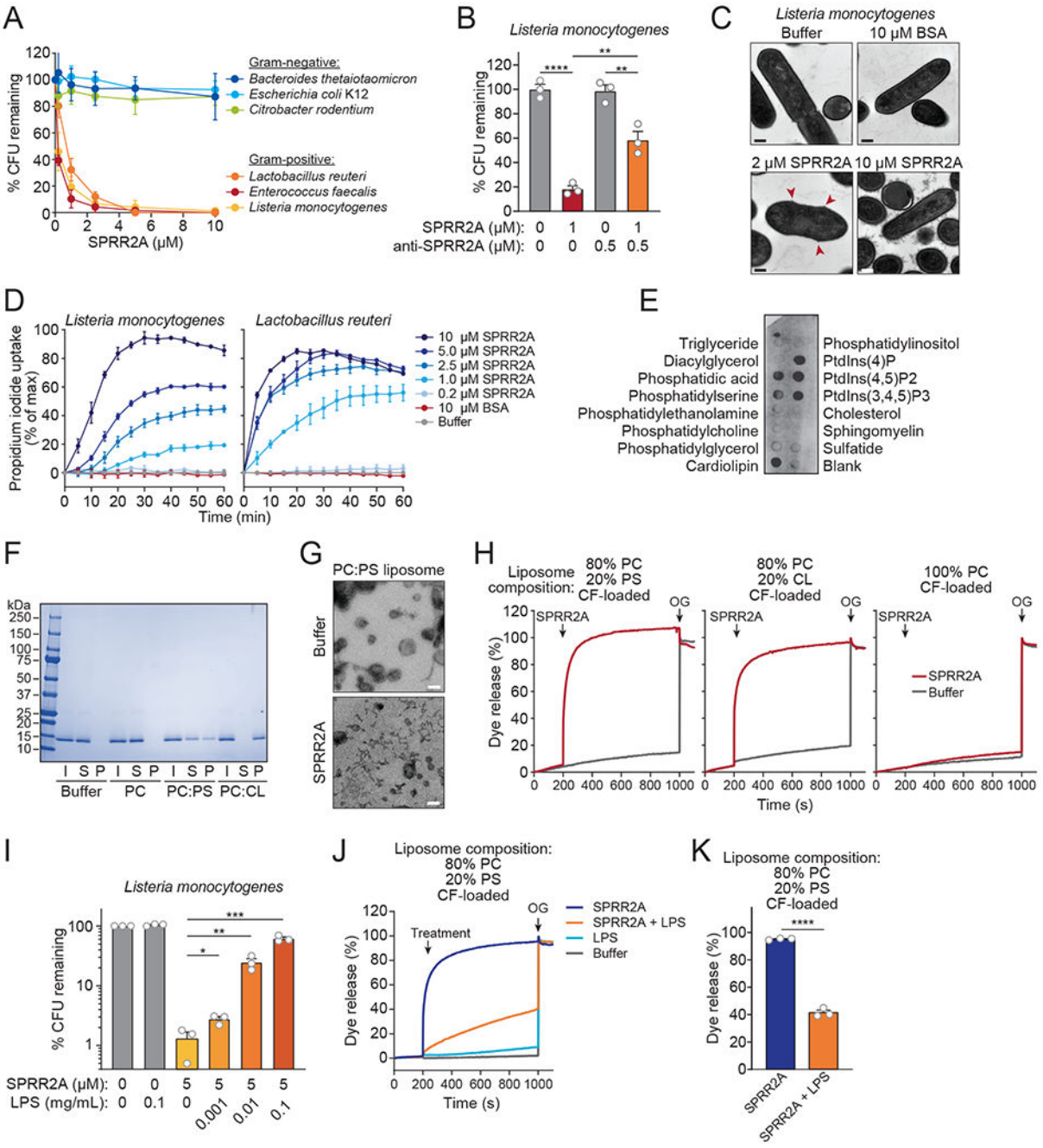

Fig. 2. SPRR2A is a bactericidal protein that targets Gram-positive bacteria by membrane permeabilization.

(A) Recombinant SPRR2A was expressed in a baculovirus expression system and purified by size exclusion chromatography. SPRR2A was added to ~10^4 CFU of log-phase bacteria for 2 hours, and surviving bacteria were enumerated by dilution plating. **(B)** SPRR2A was added to log-phase *Listeria monocytogenes* in the presence of anti-SPRR2A antibody and surviving bacteria were enumerated by dilution plating. **(C)** Transmission electron microscopy of *L. monocytogenes* after incubation with SPRR2A. Bovine serum albumin

(BSA) was used as a negative control. Examples of cell surface damage and cytoplasmic leakage are indicated with red arrowheads. Scale bars=200 nm. **(D)** *L. monocytogenes* (left) and *Lactobacillus reuteri* (right) were treated with SPRR2A or BSA as control and propidium iodide (PI) uptake was measured over 1 hour. **(E)** Membranes displaying various lipids were incubated with 1 μg/ml of SPRR2A and detected with anti-SPRR2A antibody. **(F)** SPRR2A was incubated with liposomes having the indicated lipid compositions. After ultracentrifugation, the liposome-free supernatant (S) and the liposome pellet (P) were analyzed by SDS-PAGE and Coomassie blue staining. I, input; PC, phosphatidylcholine; PS, phosphatidylserine; CL, cardiolipin. **(G)** Transmission electron microscopy of PC:PS liposomes after treatment with 5 μM SPRR2A. Scale bars=100 nm. **(H)** Carboxyfluorescein (CF)-loaded liposomes with the indicated lipid compositions were treated with 10 μM SPRR2A. Dye efflux was monitored over time and is expressed as a percentage of maximal efflux in the presence of the detergent octyl glucoside (OG). **(I)** 5 μM SPRR2A was added to log-phase *L. monocytogenes* in the presence of increasing lipopolysaccharide (LPS) concentrations. Surviving bacteria were then enumerated by dilution plating. **(J)** CF-loaded PC:PS liposomes were treated with 10 μM SPRR2A in the presence or absence of 0.2 mg/ml of LPS, and dye efflux was monitored over time and is expressed as a percentage of maximal efflux in the presence of OG. **(K)** Quantification of the results in J; n=3.
All assays were performed in triplicate and results are representative of at least two independent experiments. Means ± SEM (error bars) are plotted. *P<0.05; **P<0.01; ***P<0.001; ****P<0.0001; ns, not significant by two-tailed t test.

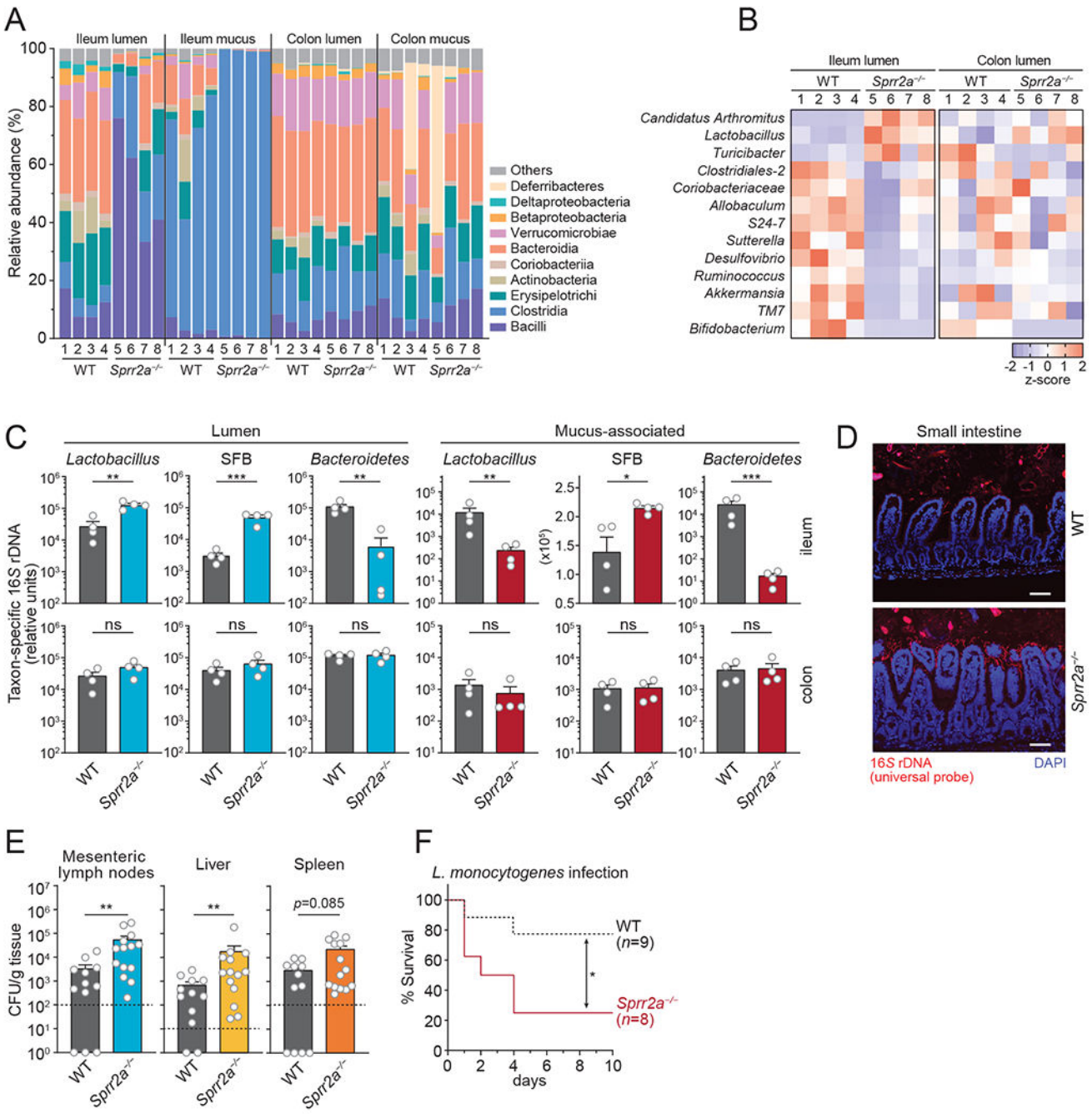

Fig. 3. Mice lacking SPRR2A have an altered intestinal microbiota and are more susceptible to *Listeria monocytogenes* infection.

(A) Male wild-type (WT) and *Sprr2a*$^{-/-}$littermates were separated at weaning and caged by genotype for 6 weeks. Intestinal mucus-associated and lumenal microbial communities were characterized by 16*S* rRNA sequencing. Relative abundances of bacterial classes in wild-type and *Sprr2a*$^{-/-}$ mice are shown. *n*=4 mice per group. **(B)** Relative abundances of bacterial genera in wild-type and *Sprr2a*$^{-/-}$ mice. **(C)** qPCR analysis of specific bacterial groups in the intestinal mucus-associated and lumenal microbial communities of wild-type

and *Sprr2a*$^{-/-}$ littermates. Values for each bacterial group are expressed relative to total 16*S* rDNA levels. **P*<0.05; ***P*<0.01; ****P*<0.001; ns, not significant by two-tailed *t* test. **(D)** Fluorescence in situ hybridization (FISH) detection of bacteria in the small intestines of wild-type and *Sprr2a*$^{-/-}$ mice. Scale bars=50 μM **(E)** 8-10-week-old wild-type (*n*=12) and *Sprr2a*$^{-/-}$ mice (*n*=14) were treated with antibiotics and orally infected with 1×10^9 CFU of log-phase *L. monocytogenes*. Liver, spleen and mesenteric lymph nodes (MLN) were collected after 24 hours and bacterial counts were determined by dilution plating. Results were pooled from three independent experiments. ***P*<0.01 by Mann–Whitney *U* test. Dotted line indicates limit of detection. **(F)** 8-10-week-old wild-type (*n*=9) and *Sprr2a*$^{-/-}$ mice (*n*=8) were orally infected with 2.5×10^9 CFU of log-phase *Listeria monocytogenes*. Survival rates were monitored over 10 days. Results were pooled from two independent experiments. **P*<0.05 by the log-rank test. WT, wild-type; SFB, segmented filamentous bacteria; CFU, colony-forming units.

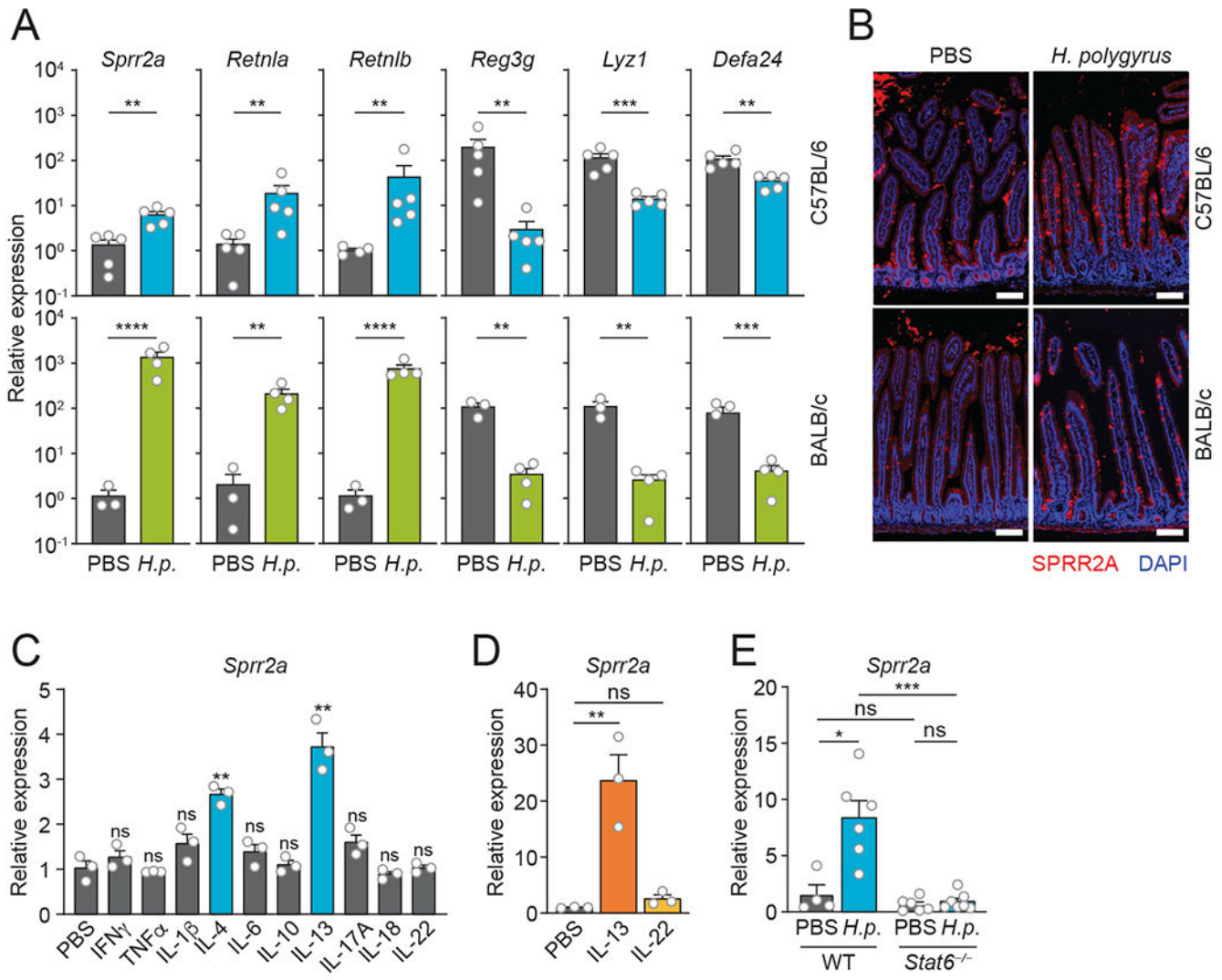

Fig. 4. SPRR2A expression is induced by type 2 cytokines during helminth infection of the intestine.

(A) Wild-type C57BL/6 (top) and BALB/c (bottom) mice were orally infected with 200 infective L3 *H. polygyrus* larvae for 2 weeks, and gene expression in the proximal jejunum was analyzed by qPCR. All values were normalized to *Gapdh* expression. **(B)** Wild-type C57BL/6 or BALB/c mice were orally infected with 200 infective L3 *H. polygyrus* larvae for 2 weeks. Control littermates were treated with PBS. SPRR2A was detected by immunofluorescence in sections of proximal jejunum. Nuclei were detected with DAPI. Scale bars=100 μm. Representative images are shown for 3-4 mice per group. (**C**) qPCR analysis of *Sprr2a* expression in small intestinal organoids derived from wild-type C57BL/6 mice treated with the indicated cytokines. Values were normalized to *Gapdh* expression. (**D**) qPCR analysis of intestinal epithelial *Sprr2a* expression in wild-type BALB/c mice intraperitoneally injected with recombinant IL-13, IL-22, or vehicle. Intestinal epithelial cells were harvested by laser-capture microdissection. Values were normalized to *Gapdh* expression. n=3 mice per group. **(E)** Wild-type and *Stat6*$^{-/-}$ mice were orally infected with

200 infective L3 *H. polygyrus* larvae, and *Sprr2a* expression in the proximal jejunum was analyzed by qPCR after 2 weeks. All values were normalized to *Gapdh* expression. Means ± SEM (error bars) are plotted. **P*<0.05; ***P*<0.01; ****P*<0.001; *****P*<0.0001; ns, not significant by two-tailed *t* test.

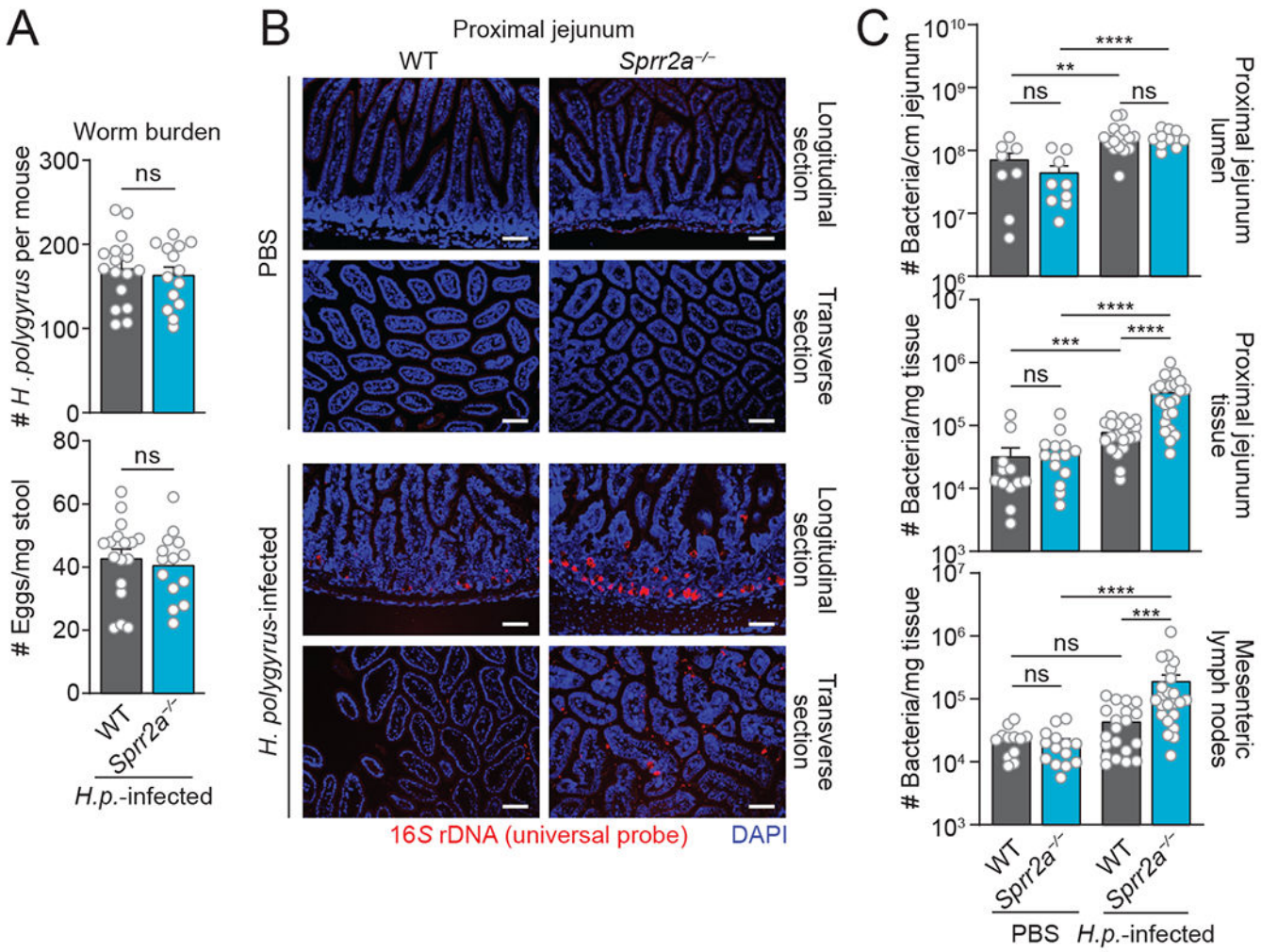

Fig. 5. SPRR2A protects against helminth-induced bacterial invasion of intestinal tissue.

(A) Wild-type and *Sprr2a*$^{-/-}$ mice were orally infected with 200 infective L3 *H. polygyrus* larvae for two weeks, and helminth burden in the intestine (upper panel) and egg numbers in the stool (lower panel) were counted. Results were pooled from two independent experiments. **(B)** Detection of bacteria by fluorescence in situ hybridization in the proximal jejunum of wild-type and *Sprr2a*$^{-/-}$ mice after *H. polygyrus* infection for 2 weeks. Nuclei were detected with DAPI. Results are representative of three independent experiments. **(C)** qPCR determination of total bacterial numbers in the proximal jejunal tissue, proximal jejunal lumen and mesenteric lymph nodes of wild-type and *Sprr2a*$^{-/-}$ mice after *H. polygyrus* infection for 2 weeks. Values were normalized to tissue weight or length. Results are from three independent experiments.

Means ± SEM (error bars) are plotted. ***P*<0.01; ****P*<0.001; *****P*<0.0001; ns, not significant by two-tailed *t* test. WT, wild-type; *H.p., Heligmosomoides polygyrus*.